The Pennsylvania State University

The Graduate School

Energy and Mineral Engineering

DUAL-PERMEABILITY DUAL-POROSITY SIMULATOR WITH PERMEABILITY EVOLUTION FOR PRODUCTION ANALYSIS OF COALBED METHANE RESERVOIR

A Thesis in

Energy and Mineral Engineering with option in

Petroleum and Natural Gas Engineering

by

Yao-Cheng Jan

Submitted in Partial Fulfillment
of the Requirements
for the Degree of

Master of Science

December 2015

The thesis of Yao-Cheng Jan was reviewed and approved* by the following:

John Yilin Wang
Associate Professor of Petroleum and Natural Gas Engineering
Thesis Advisor

Derek Elsworth
Professor of the Department of Energy and Mineral Engineering, and the Center for Geomechanics, Geofluids, and Geohazards

Shimin Liu
Assistant Professor of Energy and Mineral Engineering

Luis F. Ayala H.
Professor of Petroleum and Natural Gas Engineering
Associate Head of John and Willie Leone Family Department of Energy and Mineral Engineering for Graduate Education

*Signatures are on file in the Graduate School

ABSTRACT

The production behavior of CBM is complex and difficult to predict and analyze because it is governed by the complex physics including desorption mechanism, multi-mechanistic gas flow, initial gas content, and permeability evolution.

Numerical reservoir simulation is a reliable technique to estimate reservoir performance and production. Therefore, in this research, we developed a 3-D, 2 phase, dual porosity, dual permeability reservoir simulator with permeability evolution. By using the developed model, we also conducted a series of parametric studies to quantify the effects of desorption mechanism, adsorption capacity, multi-mechanistic flow, cleat spacing, initial gas content, permeability evolution, production pressure, and hydraulic fracture treatment.

From the results, the cumulative gas recovery will increase with adsorption capacity and initial gas content increased, lower flowing bottomhole pressure, larger diffusion coefficient, and smaller fracture spacing. We found that permeability evolution and initial gas content seem to impact CBM production more than other factors.

TABLE OF CONTENTS

LIST OF TABLES

LIST OF FIGURES

NOMENCLATURE

Roman

A_x, A_y, A_z	Cross section area	ft^2
B_g	Formation volume factor of gas	RB/Scf
B_w	Formation volume factor of water	RB/STB
C_f	Cleat volume compressibility	psi^{-1}
D	Diffusion coefficient	ft^2/Day
E	Young's modulus	psi
E_A	Modulus of the solid expansion	psi
f	Fraction range from 0-1	Fraction
$\tilde{f}$	Sorption capacity factor	Fraction
g	Gravitational acceleration	ft^2/sec
g_c	Conversion factor for g	
G	Depth from datum to the center of the block	ft
h	Thickness	ft
k	Absolute permeability	md
k_i	Initial absolute permeability	md
k_{rg}	Relative permeability for gas	fraction
k_{rw}	Relative permeability for water	fraction
K	Bulk modulus	psi
L_x, L_y, L_z	Cleat spacing in x, y, and z direction	ft
M	Constrained axial modulus	psi

M_g	Molecular weight of gas	lb/lbmol
P	Pressure	psi
P_{cgw}	Capillary pressure	psi
P_i	Initial pressure	psi
P_{wf}	Sandface pressure	psi
P_L	Langmuir pressure	psi
q_g	Gas flow rate	Scf/Day
q_{srp}	Gas sorption rate	Scf/Day
q_w	Water flow rate	STB/Day
S_g	Gas saturation	Fraction
S_{girr}	Irreducible gas saturation	fraction
S_w	Water saturation	fraction
S_{wirr}	Irreducible water saturation	fraction
r_e	Drainage radius	ft
r_w	Wellbore radius	ft
R	Gas constant (10.731)	Ft^3*psi/R-lbmol
R_{sw}	Solution gas-water ratio	Scf/STB
t	time	Day
T	temperature	R
V_b	Bulk volume	ft^3
V_E	Adsorption capacity	Scf/ft^3
V_L	Langmuir volume constant	Scf/ton

V_o	Gas molar volume	Scf/lbmol
z	Gas compressibility factor	-

Greek

α_s	Matrix coefficient for S&D model	ft^3/Scf
β	Matrix shrinkage-swelling coefficient	ft^3/Scf
ε_{exp}	Experimental strain	-
ϕ	Porosity	fraction
ϕ_i	Initial porosity	fraction
Φ_g	Flow potential of gas	psi
Φ_w	Flow potential of water	psi
γ	Grain compressibility	psi^{-1}
μ	Viscosity	cp
ρ	Coal density	ton/ft^3
ρ_g	Gas density	lb/ft^3
ρ_w	Water density	lb/ft^3
σ	Shape factor	1/ft^2
v	Poison ratio	-

Subscripts

F	Index for fracture domain

g	Index for gas phase
i	i-direction
j	j-direction
k	k-direction
M	Index for matrix domain
sc	Standard condition
up	Upstream weighting
w	Index for water phase
x	x-direction
y	y-direction
z	z-direction

ACKNOWLEDGEMENTS

First of all, I would like to thank my advisor Dr. John Yilin Wang for his guidance and patience. I had worked with Dr. Wang for about 2.5 years. Without his help, this research could not be finished. He not only taught me the professional knowledge of petroleum engineering, but also instructed me the right way for how to do and write a master thesis. I would also like to thank Dr. Elsworth and Dr. Liu to be my committee members.

Second, I would also like to thank my colleague in the Penn State 3S Laboratory, Oliver Chang, Chong Hyun Ahn, and Wenting Yue, who discuss and encourage me when we encounter challenge in research and life.

Lastly, I would like to express my deep appreciation to my parents and my brother. Thank you for them to supporting me to obtain my master degree.

Chapter 1 Introduction

Coalbed methane (CBM) reservoir, compared with the conventional gas reservoir, is an unconventional gas resources. In the past four decades, CBM has been developed due to high demand for energy from all over the world, including USA, Australia, and China. In USA, a total of 10% gas production is from CBM and the number is continue increasing. The majority of CBM production in the states had come out from three basins: The Black Warrior, San Juan, and Powder River (Figure 1). In Australia, CBM reserves are approximately 60% of the total gas reserves. In China, developments of CBM have been growing dramatically due to their high reserve which estimated to be 1,200 tcf (Chakhmakhchev 2007). Most of the CBM came from Southern Qinshui Basin (96%), while the other 4% are from Hancheng, Fuxin, Liulin, and Sanjiao areas (Benguang 2011). Development of CBM at shallow depth in China is not only an important alternative energy, but also help to avoid coalmine accidents (Meng, Zhang, and Wang 2011).

Table 1 Comparison of CBM reservoir and Conventional Gas Reservoir Characteristics (Aminian 2007)

Characteristic	Conventional	CBM
Gas Generation	Gas is generated in the source rock and then migrates into the reservoir.	Gas is generated and trapped within the coal.
Structure	Randomly-spaced Fractures	Uniformly-spaced Cleats
Gas Storage Mechanism	Compression	Adsorption
Transport Mechanism	Pressure Gradient (Darcy's Law)	Concentration Gradient (Fick's Law) and Pressure Gradient (Darcy's Law)
Production Performance	Gas rate starts high then decline. Little or no water initially. GWR decrease with time.	Gas rate increases with time then declines. Initially the production is mainly water. GWR increases with time.
Mechanical Properties	Young Modules ~ 10^6 Pore Compressibility ~10^{-6}	Young Modules ~ 10^5 Pore Compressibility ~10^{-4}

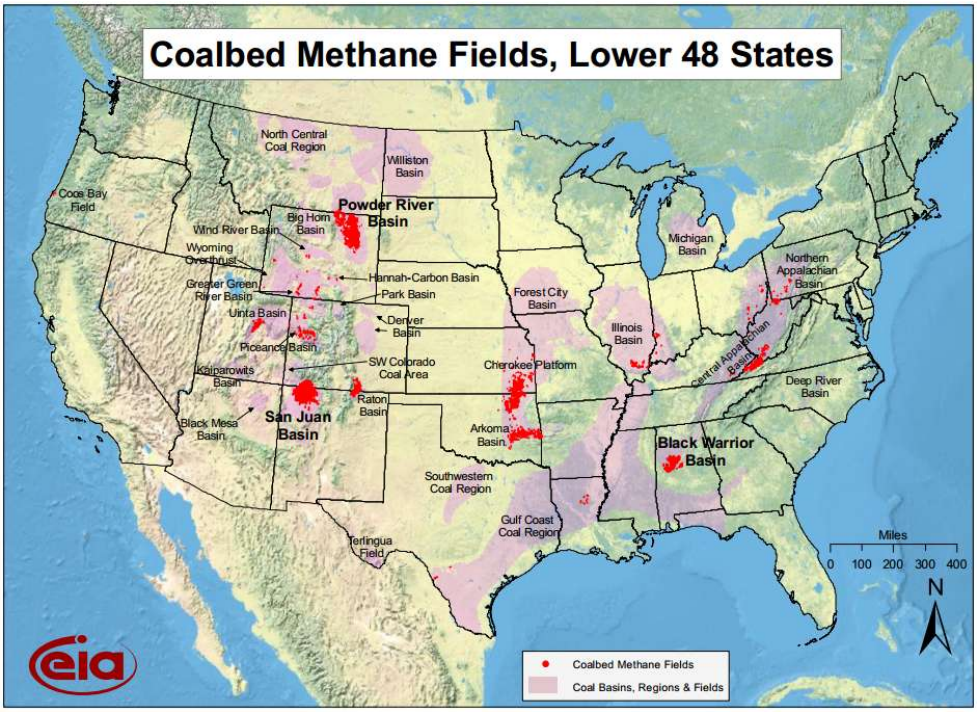

Figure 1 Map showing locations of USA basins. Source: U.S. Energy Information Administration

CBM reservoirs are naturally fractured reservoirs and could be treated as dual porosity system, which includes storage matrix domain and flow conduit fracture domain. At initial condition, methane was stored in the matrix system as adsorbed state, and the cleat system was saturated with water. After starting production, gas will release until reached the desorption pressure. Therefore, the production curve will increase at the early stage and decline after the peak gas rate. During the production, there were two competitive mechanism happened simultaneously affecting the permeability in the reservoir, which are increased effective stress due to fluid drain-out and matrix shrinkage due to gas desorption from the matrix. This phenomenon will cause the permeability change in the reservoir hence affect the gas recovery.

The production behavior of CBM is complex and difficult to predict and analyze, especially at the early stages of recovery. This is because gas production from CBM reservoirs is governed by the complex physics including desorption mechanism, multi-mechanistic gas flow, and permeability evolution as mentioned above.

Numerical reservoir simulation is one of the best method and has been proved to be a reliable technique for estimation of reservoir performance and production forecast. Therefore, in this research, we proposed a 3-D, 2 phase, dual-porosity, dual-permeability reservoir simulation model coupled with the permeability evolution module to perform the gas recovery forecast from the field. In addition, a series of parametrical studies have been conducted to evaluate the factors impacting gas production.

Chapter 2 Literature Review

The existence of methane in coal seams has been recognized for a long time. It has firstly treated as a hazard during the mining process of coal. However, it has become one of the important gas resources in the world for recent years. Since conventional gas supplies have been produced and declined for the last few years, CBM is becoming a practical and reliable substitute of energy resource for natural gas. In order to simulate the production process of CBM reservoir, we first need to have a comprehensive understanding about the characteristics of CBM including the concepts and behaviors of gas storage, flow mechanism (Darcian flow and diffusion flow), gas saturation, matrix shrinkage and swelling, and permeability evolution. Secondly, the production operation and resulting effect which called negative decline curve also need to be investigated.

2.1 CBM reservoir characterization

The following section will introduce the basic physics and mechanism of CBM reservoir. The two most important factors will be the permeability and the percentage of initial gas content. Permeability determines gas and water flow rate in the reservoir which significantly affect the gas recovery rate and the total amount. The percentage of initial gas content determined from desorption and adsorption measurements, also influences gas rate and the ultimate recoverability of gas from a reservoir (Moore 2012).

2.1.1 Gas Storage and Flow Mechanism

CBM reservoirs are dual porosity systems consisting of two porosity systems, which is permeable fracture and matrix block (Figure 2). Gas in coal can be present as free gas in fracture or as an adsorbed layer in matrix. A 1 cm^3 of coal can contain pores with an internal surface area

of $3m^2$, which is the reason that why coal could hold very large quantity of gas by gas being adsorbed onto the large pore surface area (Radlinski et al. 2004; Mares et al. 2009; Moore 2012). This is a fundamental difference between how gas is stored in conventional reservoirs versus coal reservoirs.

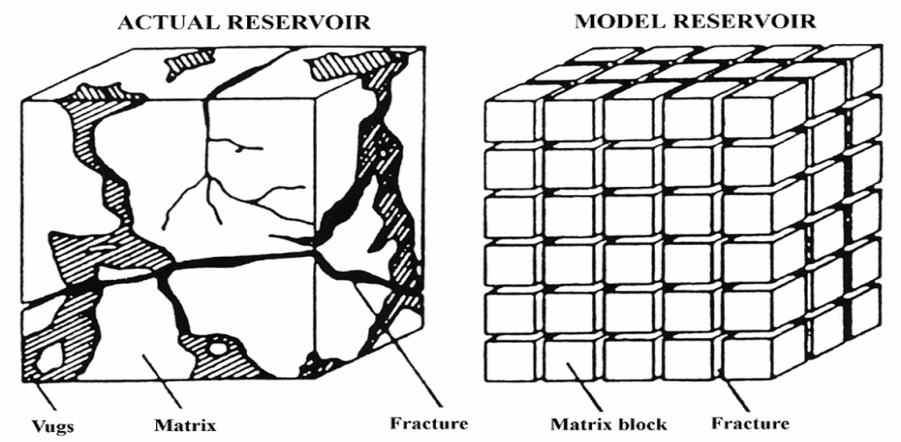

Figure 2 Idealize of a fracture system (Warren and Root 1963)

At the initial condition, the majority of the gas is stored as adsorbed state on the internal surface areas of coal matrix. The fracture network exists throughout coal seams and connects the surface area of the coal matrix. The cleat structure is initially saturated with water. When reservoir pressure decreases, water in the cleat system came out and the adsorption capacity of coal decreases causing the gas to desorb from the surface of the coal matrix and transported from the coal matrix through fracture network to the wellbore (Figure 3). Transport of gas is considered to occur under two different mechanism: (I) pressure driven flow in the cleat system under Darcy's Law, and (II) concentration-driven flow in the matrix domain under Fick's Law (Ertekin, King, and Schwerer 1986).

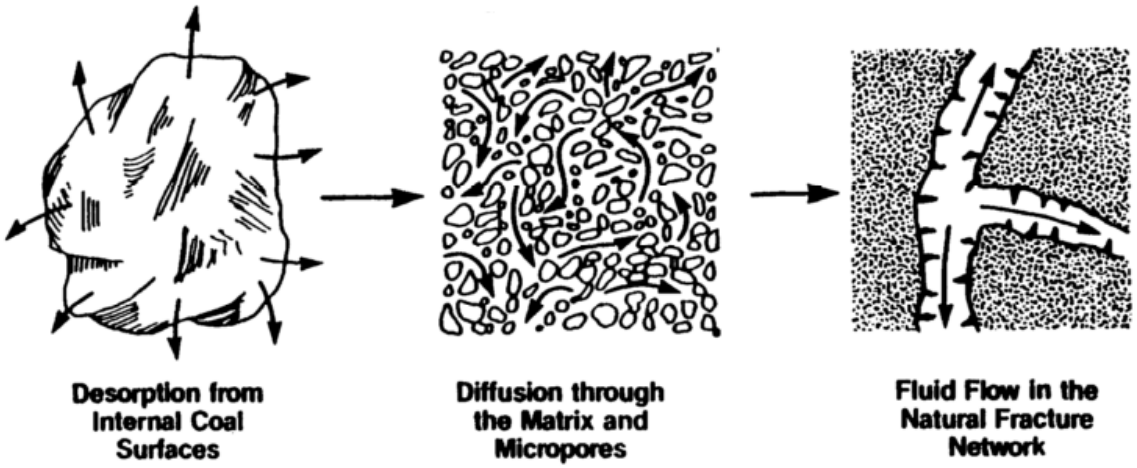

Figure 3 Processes of methane transportation in CBM reservoirs (S Harpalani and Schraufnagel 1990)

Despite there were multiple theoretical and empirical models, the Langmuir isotherm adsorption model is usually used in CBM reservoir simulation (Pan and Connell 2009). In addition, it has been indicated in several articles that only micro-pores (matrix domain) will play a significant role in adsorption, whereas macro-pores (fracture domain) acts as transport conduits (Ceglarska-Stefańska and Brzóska 1998; Ceglarsk-Stefańska and Zarębska 2002; Laubach et al. 1998; St. George and Barakat 2001).

$$V_E = \frac{V_L P}{P_L + P}$$

where V_L is the Langmuir volume constant, and P_L is the Langmuir pressure constant.

2.1.2 Diffusion

Fick's Law describes the mechanism of how gas diffusion takes place between the pores (Fick 1855).The formulation of Fick's Law could be written as follow:

$$F = D\frac{dc}{dx}$$

where F is the diffusion flux, D is the diffusion coefficient, and dC/dx represents the concentration gradient. The diffusion coefficient is emprical and is dependent on the properties of gases. Higher diffusion coefficient makes the gas transport quicker in matrix pores. The Fick's Law has three basic concepts: 1), diffusion is proportional to the concentration gradient; 2), diffusion is proportional to the amount of pore surface area; 3), speed of diffusion is inversely proportional to distance.

2.1.3 Role of Structure and Stress

The most important type of stress in CBM reservoir is the litho-static pressure, which increases with the depth in the overlying strata. The permeability decreases significantly with the depth (increased effective stress) because fractures are closed by increased effective stress (Somerton, Soylemezoglu, and Dudley 1975; Bell 2006; Sparks et al. 1995). The reduced permeability will then affect the production rate and the total amount from the reservoir (Figure 4). Horizontal stress will cause the fracture closed up. Therefore, reservoirs with low principal horizontal stress are more easier to have an artificial fracturing treatment(Moore 2012).

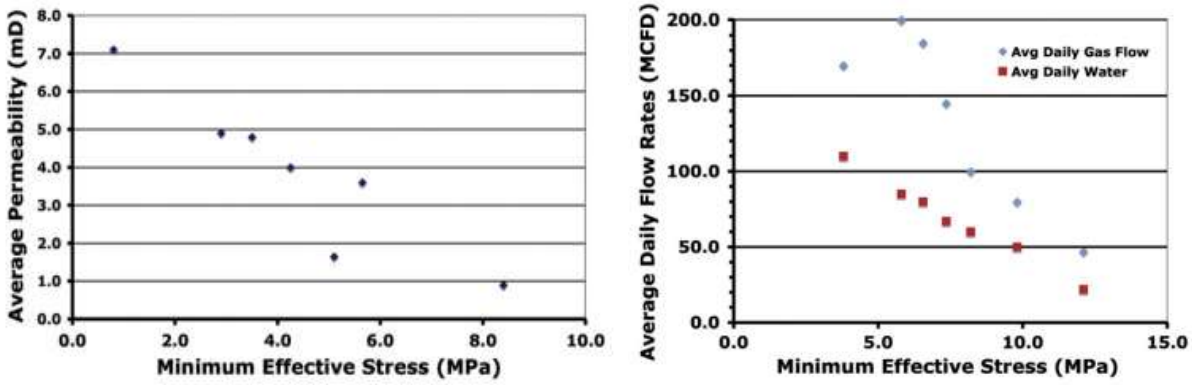

Figure 4 Minimum effective stress affect on (A) permeability and (B) gas and water production in Black Warrior Basin (Bell 2006; Sparks et al. 1995)

2.1.4 Matrix Shrinkage and Swelling- permeability evolution

Coal swelling/shrinking effect, a key component for coal reservoir permeability while primary CBM production, due to gas adsorption/desorption is a well-known phenomenon and have been the subject of many papers (Balan and Gumrah 2009; Mazumder, Scott, and Jiang 2012; Pan and Connell 2011; Pan and Connell 2012; St. George and Barakat 2001; Wang et al. 2010; Pan and Connell 2007; Liu and Harpalani 2013b). During CBM primary depletion process, two different mechanism happen at the same time with opposite effects on the reservoir permeability. 1. The fluid drain out from the field results in fluid pressure drop then increase the effective overburden stress. Hence, the reservoir becomes compressed, narrowing the cleats, which reduces the permeability and lowers the production. 2. Methane desorbs from the matrix, resulting in the coal matrix shrinks and thus enlarges the cleat, which will increase the permeability and increase the production. The shrinkage effect is related to the mechanical elastic properties of coal (Durucan, Ahsanb, and Shia 2009; Milewska-duda et al. 2000; Mavor, Owen, and Pratt 1990; Somerton, Soylemezoglu, and Dudley 1975; St. George and Barakat 2001; Yao et al. 2009). Therefore, stress sensitivity and matrix shrinkage are the two competitive factors changing absolute permeability variation, which results in problems for reservoir performance analysis, production prediction, reserve estimation and development optimization (Tao et al. 2012).

Permeability defines the level of transportability of gas, which determined the migration and output ability of CBM reservoirs. Based on the effects mentioned above, several permeability models had been proposed to illustrate the effect of shrinkage and swelling on the permeability changes in coal. Palmer and Mansoori (1998) (P&M) developed a strain-based model which was derived using the cubic relationship between permeability and porosity and the equation of

elasticity for strain in porous rock. This model was developed based on a theoretical formulation for stress-dependent permeability of coalbeds that includes the effects of cleat compression and matrix shrinkage. Shi and Durucan (2005) (S&D) proposed a stress-based model using an exponential relationship between the ratio of permeability and the change in effective stress caused by volumetric deformation and cleat compressibility. An assumption that volumetric-shrinkage strain is correlated directly to the amount of gas desorbed is implemented. Thararoop, et al (Thararoop, Karpyn, and Ertekin 2009) proposed a model that they believed the previous models did not account for water present in the matrix domain. As the moisture content in the matrix increase, the gas sorption capacity of coal matrix will decrease. Hence, they incorporated a sorption factor $\tilde{f}$. Liu et.al (Liu and Harpalani 2013a) theoretically developed a new volumetric strain approach based on the surface energy. They believed that the volumetric strain in P&M and S&D models could not been analogues as the thermal expansion. Therefore, they replaced that term with their new approached and have validated it to match with the experiment data. Table 2 presents the equations of the existing coal shrinkage and swelling models discussed above.

Model	**Equation**
P&M	$\frac{k}{k_i} = \left(\frac{\phi}{\phi_i}\right)^3 = \left[1 + \frac{\tilde{c}_m}{\phi_i}(p - p_i) + \frac{\varepsilon_i}{\phi_i}\left[\frac{K}{M} - 1\right]\left(\frac{p}{p_L+p} - \frac{p_i}{p_L+p_i}\right)\right]^3$ Where $\tilde{c}_m = \frac{1}{M} - \left[\frac{K}{M} + f - 1\right]\gamma$
S&D	$\frac{k}{k_i} = \exp\left\{-3C_f\left[-\frac{\nu}{1-\nu}(p - p_i) + \frac{E\alpha_S V_L}{3(1-\nu)}\left(\frac{p}{p_L+p} - \frac{p_i}{p_L+p_i}\right)\right]\right\}$
Thararoop	$\frac{k}{k_i} = \left(\frac{\phi}{\phi_i}\right)^3 = \left\{e^{C_p(p-p_i)} + \frac{\tilde{f}\beta V_m}{\phi_i}\left(\frac{p_i}{p_L+p_i} - \frac{p}{p_L+p}\right)\right\}^3$

P&M&Liu	$\frac{k}{k_i} = \left(\frac{\phi}{\phi_i}\right)^3 = \left[1 + \frac{\widetilde{C_m}}{\phi_i}(p - p_i) + \frac{1}{\phi_i}\left[\frac{K}{M} - 1\right]\Delta\varepsilon\right]^3$ Where $\Delta\varepsilon = \frac{3V_L\rho RT}{\mathrm{E_A V_o}}\int_{p_1}^{p_2}\frac{1}{P_L+P}dP$
S&D&Liu	$\frac{k}{k_i} = exp\left\{-3C_f\left[-\frac{v}{1-v}(p - p_i) + \frac{E}{3(1-v)}\Delta\varepsilon\right]\right\}$ Where $\Delta\varepsilon = \frac{3V_L\rho RT}{\mathrm{E_A V_o}}\int_{p_1}^{p_2}\frac{1}{P_L+P}dP$

Table 2 equation of the existing coal shrinkage and swelling models

2.1.5 Initial gas content

The degree of gas saturation is arguably the second most important parameter (after permeability) in a CBM reservoir. Without sufficient gas saturation, gas flow will not be economic. A general rule of thumb in the CBM industry is that reservoirs need to have greater than 70% initial gas content in order to be economic (Moore 2012). Figure 5 illustrate that with higher initial gas content, reservoir need less time to be de-pressurized to reach the desorption pressure. Until reaching the desorption pressure, gas will not release from the internal surface of the pores to fracture. Therefore, higher initial gas content will result in higher total gas recovery.

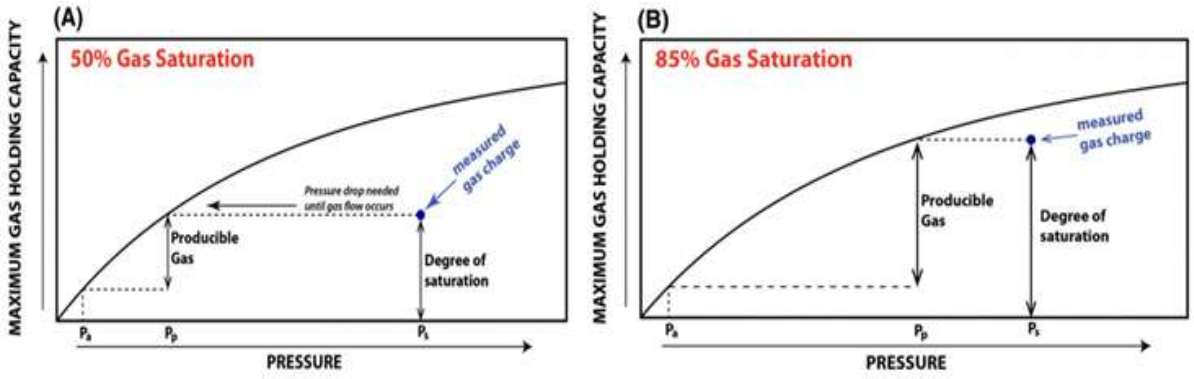

Figure 5 Comparison of effect of two different initial gas content on de-pressurisation and predicted ultimate gas production. (A) 50% initial gas content and (B) 85% initial gas content

2.2 Production operation

Most CBM reservoirs produce only water at the beginning because the cleats in the reservoir are filled with water. Typically, water must be produced continuously from coal seams to reduce reservoir pressure until reaching desorption pressure, where gas started to release from the matrix. The cost to treat and dispose the produced water can be an economic issue of a CBM project. As the desorption process continues, gas saturation within the cleat system increases and flow of methane became more dominant. Therefore, water rate decline rapidly and gas rate increasing until reach the peak value. Figure 6 shows a typical CBM production profile. The phenomenon that gas rate increase at early time then decrease called 'negative decline', which is commonly seen in CBM reservoir.

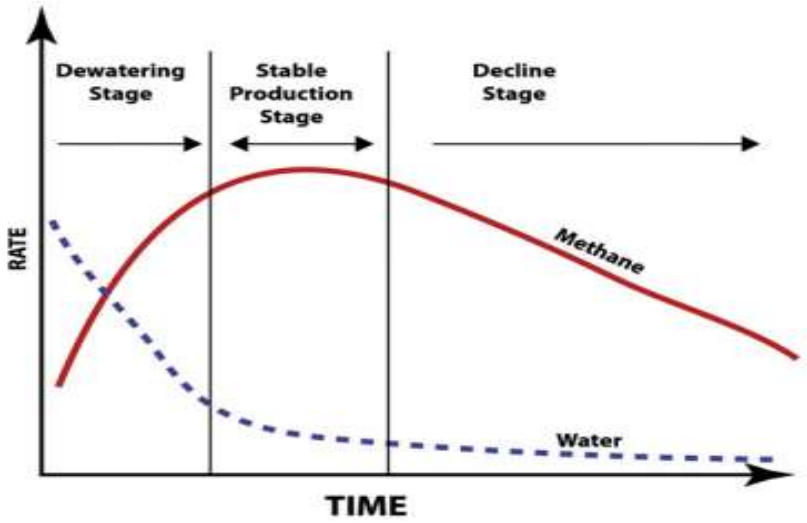

Figure 6 CBM production profile showing the different phases of production (Moore 2012)

2.2.1 Dewatering operation

Furthermore, certain engineering factors, such as the dewatering rate. The dewatering rate has a significant impact on the pressure reduction rate, causing both stress sensitivity and matrix shrinkage; therefore, it can either damage or improve the absolute permeability of coal reservoirs. If the dewatering rate is low, the CBM desorption rate will be low and therefore unfavorable for

matrix shrinkage. Here, stress sensitivity always plays a leading role. When the dewatering rate is high, the CBM desorption rate will be high and thus favorable for matrix shrinkage, which may play a leading role in coal seams with a large elastic modulus. These observations indicate that an optimized dewatering rate must be maintained during the development process to avoid reservoir damage and to promote matrix shrinkage) and bottom-hole pressure (the bottom hole pressure should be controlled; it cannot simply be reduced to obtain a large production pressure difference without considering the potential impacts of stress sensitivity and gas locking), are also important. Most of these factors first change the coal reservoir permeability and then the CBM production. In the early production period of a CBM well, only water is produced. To shorten this single-phase water period and achieve gas breakthrough more quickly, a relatively high drainage speed is favorable. However, when the well starts to produce gas, the dewatering rate should be decreased slowly and steadily, especially after the gas peak appears.

2.3 Problem statement

The production behavior of CBM is a complex physics including desorption, multi-mechanistic gas flow, initial gas content, and permeability evolution. Although it had been studied for recent years, we still lack the method to accurately quantify the impact factors of gas recovery during the primary depletion stage.

The procedures of the research are as follow:

1. Had a comprehensive literature review for the mechanism and phenomenon of CBM production.
2. Developed the mathematical formulation to capture and couple all the physics affecting production.

3. Programmed the mathematical formulation into MATLAB and validate with the commercial software.
4. Conducted a series of parametrical studies to investigate the impact factors of gas recovery

Chapter 3 Mathematical Model Development

The governing equation used in the model will be derived in detail in this chapter. It is a multi-mechanistic two-phase flow model in a dual-porosity, dual permeability system with a module to capture the physics of permeability evolution. The governing equations in the model are developed for gas and water flow in two domains, which are fracture domain and matrix domain. The micro-pores in matrix domain is the primary storage part and the fracture domain is the main conduit part for gas and water transport from the reservoir to the wellbore. The gas flow in both fracture and matrix domain are treated as a multi-mechanistic flow while the water flow is assumed to be Darcian flow only.

3.1 Governing Equations

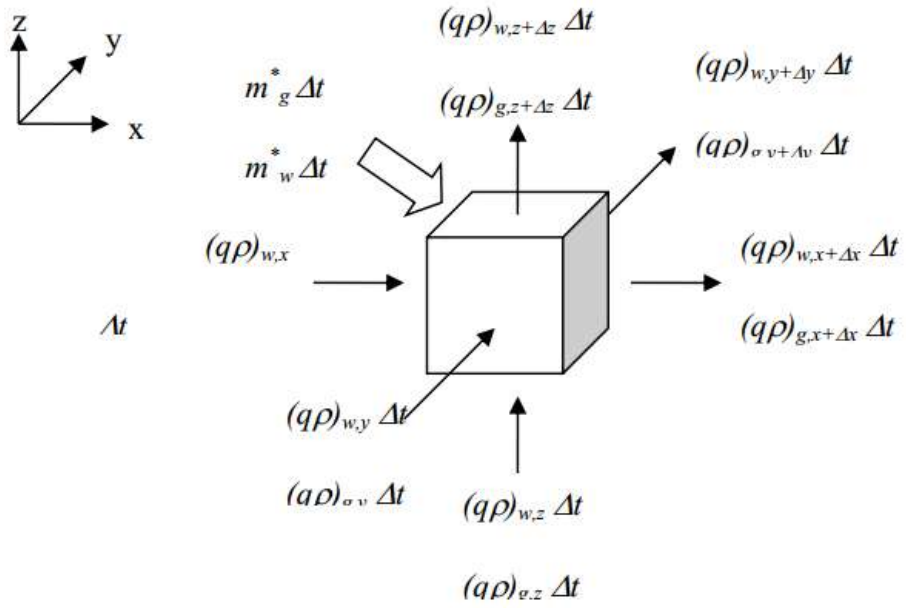

Figure 7 Simple plot of finite volume of a reservoir block over time interval Δt

$$[mass\ in] - [mass\ out] + [source\ or\ sink] = [mass\ change] \tag{3.1}$$

Fluid transport in both fracture and matrix domain obey the principle of mass conservation (equation 3.1). The principle of mass conservation has the assumption that there is no chemical reaction take place which will gain or loss mass within the system. The fluid flow in porous media is based on Darcy's Law which means all the assumptions inherent in the law applies to the model. In order to formulate the equations, the simulated reservoir first need to be assigned an idealized structure grids. The coordinate systems for the grids we used to develop the model is Cartesian coordinates, but it could easily transform the equations to spheres or cylinder coordinates.

Based on the assumption above and the equation 3.1 we can have the mass balance equation in fracture domain of phase 'p' for a finite volume of a reservoir block over a time interval Δt (equation 3.2).

$$\left[\left(M_{p,F}\right)_{x+\Delta x}\Delta t + \left(M_{p,F}\right)_{y+\Delta y}\Delta t + \left(M_{p,F}\right)_{y+\Delta y}\Delta t\right] - \left[\left(M_{p,F}\right)_{x}\Delta t + \left(M_{p,F}\right)_{y}\Delta t + \left(M_{p,F}\right)_{y}\Delta t\right] - Q^{*}_{p,F}\Delta t + \left[\Delta x\Delta y\Delta z\phi\left(S_{p,F}\rho_{p}\right)\right]_{t+\Delta t} - \left[\Delta x\Delta y\Delta z\phi\left(S_{p,F}\rho_{p}\right)\right]_{t} = 0 \quad (3.2)$$

where we have the mass in/out for

$$M_{p,F_x} = m_{p,F_x}\Delta y\Delta z\,, M_{p,F_y} = m_{p,F_y}\Delta \mathrm{x}\Delta z\,, M_{p,F_z} = m_{p,F_z}\Delta \mathrm{x}\Delta \mathrm{y} \quad (3.3)$$

and the mass flux could be written as

$$m_{p,F_x} = \rho_p v_{p,F_x}\,, m_{p,F_y} = \rho_p v_{p,F_y}\,, m_{p,F_z} = \rho_p v_{p,F_z} \quad (3.4)$$

Therefore, substituting equation 3.3 and 3.4 to equation 3.2, and dividing by Δt, we can get

$$-\left[\left(\rho_p v_{p,F_x}A_x\right)_{x+\Delta x} - \left(\rho_p v_{p,F_x}A_x\right)_{x}\right] - \left[\left(\rho_p v_{p,F_y}A_y\right)_{y+\Delta y} - \left(\rho_p v_{p,F_y}A_y\right)_{y}\right]$$

$$-\left[\left(\rho_p v_{p,F_z} A_z\right)_{z+\Delta z} - \left(\rho_p v_{p,F_z} A_z\right)_z\right] + Q^*_{p,F} = \left(\phi_F V_b \frac{S_{p,F}\rho_p}{\Delta t}\right)_{t+\Delta t} - \left(\phi_F V_b \frac{S_{p,F}\rho_p}{\Delta t}\right)_t \quad (3.5)$$

The differential form of mass balance equation will become

$$-\frac{\partial}{\partial x}\left(\rho_p v_{p,F_x} A_x\right)\Delta x - \frac{\partial}{\partial y}\left(\rho_p v_{p,F_y} A_y\right)\Delta y - \frac{\partial}{\partial z}\left(\rho_p v_{p,F_z} A_z\right)\Delta z + Q^*_{p,F} = V_b \frac{\partial}{\partial t}\left(\phi_F \rho_p S_{p,F}\right) \quad (3.6)$$

For 3-dimensional, multi-phase flow, the Darcy's Law for phase 'p' is

$$\overrightarrow{v_{p,F}} = -5.615 \frac{k k_{rp}}{\mu_F} \vec{\nabla} \Phi_{p,F} \quad (3.7)$$

In addition, the density of phase 'p' could be written as the density at surface condition and formation volume factor.

$$\rho_p = \frac{\rho_{p_{SC}}}{B_p} \quad (3.8)$$

Substituting equation 3.7 and 3.8 to equation 3.6, the flow equation in fracture domain for phase 'p' could be written as follow

$$\frac{\partial}{\partial x}\left(\frac{A_x k_x k_{rp}}{\mu_p B_p}\frac{\partial \Phi_{p,F}}{\partial x}\right)\Delta x + \frac{\partial}{\partial y}\left(\frac{A_y k_y k_{rp}}{\mu_p B_p}\frac{\partial \Phi_{p,F}}{\partial y}\right)\Delta y + \frac{\partial}{\partial z}\left(\frac{A_z k_z k_{rp}}{\mu_p B_p}\frac{\partial \Phi_{p,F}}{\partial z}\right)\Delta z + Q^*_{p,F} = \frac{1}{5.615}\frac{\partial}{\partial t}\left(\frac{\phi_F V_b S_{p,F}}{B_p}\right) \quad (3.9)$$

In the model, the total mass of phase 'p' generated or depleted from the fracture ($Q_{p,F}$) is the summation of mass injected or produced at a well ($Q_{1,p,F}$) and mass loss or gained from a matrix block ($Q_{2,p,F}$).

$$Q^*_{p,F} = Q_{1,p,F} + Q_{2,p,F} \quad (3.10)$$

In gas phase

$$Q_{1,g,F}\left(\frac{lb}{D}\right) = \rho_{g_{SC}}\left(\frac{lb}{scf}\right) q_g \left(\frac{scf}{D}\right) \quad (3.11)$$

$$Q_{2,g,F}\left(\frac{lb}{D}\right) = \rho_{g_{SC}}\left(\frac{lb}{scf}\right)\Gamma_{g,F}\left(\frac{scf}{D}\right) \tag{3.12}$$

In water phase

$$Q_{1,w,F}\left(\frac{lb}{D}\right) = 5.615\left(\frac{scf}{STB}\right)\rho_{w_{SC}}\left(\frac{lb}{scf}\right)q_w\left(\frac{STB}{D}\right) \tag{3.13}$$

$$Q_{2,w,F} = 5.615\left(\frac{scf}{STB}\right)\rho_{w_{SC}}\left(\frac{lb}{scf}\right)\Gamma_{w,F}\left(\frac{STB}{D}\right) \tag{3.14}$$

Besides, the flow equation for gas need to incorporate the diffusion flow which based on the Fick's Law and the gas dissolve in water phase. So the gas flow equation in fracture domain is

$$\begin{aligned}
&\frac{\partial}{\partial x}\left(\frac{D_F\phi_F S_{g,F}A_x}{5.615}\frac{\partial}{\partial x}\left(\frac{S_{g,F}}{B_{g,F}}\right) + \frac{A_x k_x k_{rg,F}}{\mu_g B_{g,F}}\frac{\partial \Phi_{g,F}}{\partial x} + R_{sw,F}\frac{A_x k_x k_{rw,F}}{\mu_w B_{w,F}}\frac{\partial \Phi_{w,F}}{\partial x}\right)\Delta x \\
&+ \frac{\partial}{\partial y}\left(\frac{D_F\phi_F S_{g,F}A_y}{5.615}\frac{\partial}{\partial y}\left(\frac{S_{g,F}}{B_{g,F}}\right) + \frac{A_y k_y k_{rg,F}}{\mu_g B_{g,F}}\frac{\partial \Phi_{g,F}}{\partial y} + R_{sw,F}\frac{A_y k_y k_{rw,F}}{\mu_w B_{w,F}}\frac{\partial \Phi_{w,F}}{\partial y}\right)\Delta \mathrm{y} \\
&+ \frac{\partial}{\partial z}\left(\frac{D_F\phi_F S_{g,F}A_z}{5.615}\frac{\partial}{\partial z}\left(\frac{S_{g,F}}{B_{g,F}}\right) + \frac{A_z k_z k_{rg,F}}{\mu_g B_{g,F}}\frac{\partial \Phi_{g,F}}{\partial z} + R_{sw,F}\frac{A_z k_z k_{rw,F}}{\mu_w B_{w,F}}\frac{\partial \Phi_{w,F}}{\partial z}\right)\Delta \mathrm{z} \\
&+ \Gamma_{g,F} + q_g + R_{sw,F}q_{w,F} = \frac{1}{5.615}\frac{\partial}{\partial t}\left(\frac{\phi_F V_b S_{g,F}}{B_{g,F}} + R_{sw}\frac{\phi_F V_b S_{w,F}}{B_{w,F}}\right)
\end{aligned} \tag{3.15}$$

The water flow equation in fracture domain, which is Darcian flow only, will be

$$\begin{aligned}
&\frac{\partial}{\partial x}\left(\frac{A_x k_x k_{rw,F}}{\mu_w B_{w,F}}\frac{\partial \Phi_{w,F}}{\partial x}\right)\Delta x + \frac{\partial}{\partial y}\left(\frac{A_y k_y k_{rw,F}}{\mu_w B_{w,F}}\frac{\partial \Phi_{w,F}}{\partial y}\right)\Delta \mathrm{y} + \frac{\partial}{\partial z}\left(\frac{A_z k_z k_{rw,F}}{\mu_w B_{w,F}}\frac{\partial \Phi_{w,F}}{\partial z}\right)\Delta \mathrm{z} \\
&+ \Gamma_{w,F} + q_w = \frac{1}{5.615}\frac{\partial}{\partial t}\left(\frac{\phi_F V_b S_{w,F}}{B_{w,F}}\right)
\end{aligned} \tag{3.16}$$

where the potential term which depth is assumed positive downward from the datum plane could be written as

$$\Phi_{g,F} = P_{g,F} - \frac{1}{144}\frac{g}{g_c}\rho_g G \tag{3.17}$$

$$\Phi_{w,F} = P_{w,F} - \frac{1}{144}\frac{g}{g_c}\rho_w G \tag{3.18}$$

In matrix domain, the governing equations are also derived under the conservation of mass. The gas equation including two parts, one is the gas flow between fracture and matrix system, and one is the gas desorb from the matrix. Since the conservation of mass, the mass flow out from the matrix to fracture will equal to the mass flow into fracture from the matrix.

$$\Gamma_{g,M} = -\Gamma_{g,F} = \frac{1}{5.615}\frac{\partial}{\partial t}\left[\frac{V_b\phi_M S_{g,M}}{B_{g,M}} + R_{sw,M}\frac{V_b\phi_M S_{w,M}}{B_{w,M}}\right] + q_{srp} \tag{3.19}$$

The governing equation for water phase is the flow between fracture and matrix only ($\Gamma_{w,F}$).

$$\Gamma_{w,M} = -\Gamma_{w,F} = \frac{1}{5.615}\frac{\partial}{\partial t}\left[\frac{V_b\phi_M S_{w,M}}{B_{w,M}}\right] \tag{3.20}$$

Auxiliary Equations

Since we assume there is only one component for the gas which is methane, so there are total 8 unknown variables in a grid block need to be solved in the system of equations, which are $P_{g,F}$, $P_{w,F}$, $P_{g,M}$, $P_{w,M}$, $S_{g,F}$, $S_{w,F}$, $S_{g,M}$, $S_{w,M}$. Therefore, we need 8 equations to solve for them. A total of 4 equations could be obtained from section 3.1 which are equation (3.15), (3.16), (3.19), and (3.20). The remaining 4 equations could get from capillary pressure and saturation constrains for both fracture and matrix domain.

Capillary pressure constrains

$$P_{cgw,F} = P_{g,F} - P_{w,F} \tag{3.21}$$

$$P_{cgw,M} = P_{g,M} - P_{w,M} \tag{3.22}$$

Saturation constrains

Summation of gas and water saturation in each domain is unity.

$$S_{g,F} + S_{w,F} = 1 \tag{3.23}$$

$$S_{g,M} + S_{w,M} = 1 \tag{3.24}$$

3.2 Finite-Difference Approximations

The partial differential equations for gas and water flow in the fracture and matrix system had been derived in section 3.1 which contain derivatives with respect to time and space. The derivatives could be approximated by finite difference method or finite element method, which are the two most commonly used discretization method in oil industry. In our model, we used finite difference method with central difference for space (equation 3.25) and forward difference for time (equation 3.26). In order to use this method, a finite difference grid must superimposed on the idealized grid blocks. In this work, we used a body-centered grid system with Cartesian coordinates. In addition, the following residual forms of approximation equations were written in 1-D system to simplify the equations.

$$\frac{\partial^2 p}{\partial x^2} = \frac{p_{i+1} - 2p_i + p_{i-1}}{(\Delta x)^2} \tag{3.25}$$

$$\frac{\partial p}{\partial t} = \frac{p_i^{n+1} - p_i^n}{\Delta t} \tag{3.26}$$

Gas in fracture domain:

$$R_{g,F}\Big|_i^{n+1} = \frac{D_F \phi_F S_{g,F} A_x}{5.615\Delta x}\Big|_{i+\frac{1}{2}} \left[\left(\frac{S_{g,F}}{B_{g,F}}\right)_{i+1}^{n+1} - \left(\frac{S_{g,F}}{B_{g,F}}\right)_{i}^{n+1}\right]$$

$$- \frac{D_F \phi_F S_{g,F} A_x}{5.615\Delta x}\Big|_{i-\frac{1}{2}} \left[\left(\frac{S_{g,F}}{B_{g,F}}\right)_{i}^{n+1} - \left(\frac{S_{g,F}}{B_{g,F}}\right)_{i-1}^{n+1}\right]$$

$$+ \frac{A_x}{\Delta x}\Big|_{i+\frac{1}{2}} k_{x,F}\Big|_{i+\frac{1}{2}}^{n+1} \frac{1}{\mu_g B_{g,F}}\Big|_{i+\frac{1}{2}}^{n+1} k_{rg,F}\Big|_{up}^{n+1} \left(\Phi_{g,F}\Big|_{i+1}^{n+1} - \Phi_{g,F}\Big|_{i}^{n+1}\right)$$

$$- \frac{A_x}{\Delta x}\Big|_{i-\frac{1}{2}} k_{x,F}\Big|_{i-\frac{1}{2}}^{n+1} \frac{1}{\mu_g B_{g,F}}\Big|_{i-\frac{1}{2}}^{n+1} k_{rg,F}\Big|_{up}^{n+1} \left(\Phi_{g,F}\Big|_{i}^{n+1} - \Phi_{g,F}\Big|_{i-1}^{n+1}\right)$$

$$+ \frac{A_x}{\Delta x}\Big|_{i+\frac{1}{2}} k_{x,F}\Big|_{i+\frac{1}{2}}^{n+1} \frac{R_{sw,F}}{\mu_w B_{w,F}}\Big|_{i+\frac{1}{2}}^{n+1} k_{rw,F}\Big|_{up}^{n+1} \left(\Phi_{w,F}\Big|_{i+1}^{n+1} - \Phi_{w,F}\Big|_{i}^{n+1}\right)$$

$$- \frac{A_x}{\Delta x}\Big|_{i-\frac{1}{2}} k_{x,F}\Big|_{i-\frac{1}{2}}^{n+1} \frac{R_{sw,F}}{\mu_w B_{w,F}}\Big|_{i-\frac{1}{2}}^{n+1} k_{rw,F}\Big|_{up}^{n+1} \left(\Phi_{w,F}\Big|_{i}^{n+1} - \Phi_{w,F}\Big|_{i-1}^{n+1}\right) + \Gamma_{g,F}\Big|_i^{n+1}$$

$$+ q_g\Big|_i^{n+1} + R_{sw,F} q_w\Big|_i^{n+1} - \frac{1}{5.615\Delta t}\left[\left(\frac{V_b \phi_F S_{g,F}}{B_{g,F}}\right)_i^{n+1} + \left(R_{sw}\frac{V_b \phi_F S_{w,F}}{B_{w,F}}\right)_i^{n+1}\right]$$

$$+ \frac{1}{5.615\Delta t}\left[\left(\frac{V_b \phi_F S_{g,F}}{B_{g,F}}\right)_i^{n} + \left(R_{sw}\frac{V_b \phi_F S_{w,F}}{B_{w,F}}\right)_i^{n}\right]$$

(3.27)

Water in fracture domain:

$$R_{w,F}\big|_i^{n+1} = \frac{A_x}{\Delta x}\Big|_{i+\frac{1}{2}} k_{x,F}\big|_{i+\frac{1}{2}}^{n+1} \frac{1}{\mu_w B_{w,F}}\Big|_{i+\frac{1}{2}}^{n+1} k_{rw,F}\big|_{up}^{n+1} \left(\Phi_{w,F}\big|_{i+1}^{n+1} - \Phi_{w,F}\big|_i^{n+1}\right)$$

$$- \frac{A_x}{\Delta x}\Big|_{i-\frac{1}{2}} k_{x,F}\big|_{i-\frac{1}{2}}^{n+1} \frac{1}{\mu_w B_{w,F}}\Big|_{i-\frac{1}{2}}^{n+1} k_{rw,F}\big|_{up}^{n+1} \left(\Phi_{w,F}\big|_i^{n+1} - \Phi_{w,F}\big|_{i-1}^{n+1}\right) + \Gamma_{w,F}\big|_i^{n+1}$$

$$+ q_w\big|_i^{n+1} - \frac{1}{5.615\Delta t}\left(\frac{V_b \phi_F S_{w,F}}{B_{w,F}}\right)_i^{n+1} + \frac{1}{5.615\Delta t}\left(\frac{V_b \phi_F S_{w,F}}{B_{w,F}}\right)_i^{n} \tag{3.28}$$

Gas in matrix domain:

$$R_{g,M}\big|_i^{n+1} = \Gamma_{g,M}\big|_i^{n+1} - q_{srp}\big|_i^{n+1} - \frac{1}{5.615\Delta t}\left[\left(\frac{V_b \phi_F S_{g,F}}{B_{g,F}}\right)_i^{n+1} + \left(R_{sw}\frac{V_b \phi_F S_{w,F}}{B_{w,F}}\right)_i^{n+1}\right] +$$

$$\frac{1}{5.615\Delta t}\left[\left(\frac{V_b \phi_F S_{g,F}}{B_{g,F}}\right)_i^{n} + \left(R_{sw}\frac{V_b \phi_F S_{w,F}}{B_{w,F}}\right)_i^{n}\right] \tag{3.29}$$

Water in matrix domain:

$$R_{w,M}\big|_i^{n+1} = \Gamma_{w,M}\big|_i^{n+1} - \frac{1}{5.615\Delta t}\left(\frac{V_b \phi_F S_{w,F}}{B_{w,F}}\right)_i^{n+1} + \frac{1}{5.615\Delta t}\left(\frac{V_b \phi_F S_{w,F}}{B_{w,F}}\right)_i^{n} \tag{3.30}$$

The superscripts n+1 is the term indicates the new time step while n is the previous time step.

3.3 Transmissibility Terms

The transmissibility terms are the fluid movement between two neighboring grid blocks, which means we have to calculate the property coefficients at the interface of these two blocks. The terms generally contain three different groups of coefficients, which are grid block properties, fluid properties and rock properties. Taking the term from equation (3.27) at the interface between grid block i and i+1 in the fracture system for Darcian flow as an example.

$$\left[\frac{A_x}{\Delta x}\Big|_{i+\frac{1}{2}} k_{x,F}\Big|_{i+\frac{1}{2}}^{n+1}\right]\left[\frac{1}{\mu_g B_{g,F}}\Big|_{i+\frac{1}{2}}^{n+1}\right]\left[k_{rg,F}\Big|_{up}^{n+1}\right]$$

The first term, $\left[\frac{A_x}{\Delta x}\Big|_{i+\frac{1}{2}} k_{x,F}\Big|_{i+\frac{1}{2}}^{n+1}\right]$, is the linear term related to the dimension of the grids (constant) and rock property which is the permeability of the fracture. The permeability is a function of pressure as it changes due to the coal shrinkage and swelling effects. This first term could be calculated by harmonic average.

$$\left[\frac{A_x}{\Delta x}\Big|_{i+\frac{1}{2}} k_{x,F}\Big|_{i+\frac{1}{2}}^{n+1}\right] = \frac{2A_x|_i A_x|_{i+1} k_{x,F}|_i^{n+1} k_{x,F}|_{i+1}^{n+1}}{A_x|_i k_{x,F}|_i^{n+1}\Delta x|_{i+1} + A_x|_{i+1} k_{x,F}|_{i+1}^{n+1}\Delta x|_i} \tag{3.31}$$

The second term, $\left[\frac{1}{\mu_g B_{g,F}}\Big|_{i+\frac{1}{2}}^{n+1}\right]$, is the weakly non-linear term of fluid properties (viscosity and formation volume factor) and pressure. Each part in the term could be calculated by arithmetic average.

$$\left[\frac{1}{\mu_g B_{g,F}}\Big|_{i+\frac{1}{2}}^{n+1}\right] = \left[0.5\left(\mu_g|_i^{n+1} + \mu_g|_{i+1}^{n+1}\right) 0.5\left(B_{g,F}|_i^{n+1} + B_{g,F}|_{i+1}^{n+1}\right)\right]^{-1} \tag{3.32}$$

The third term, $\left[k_{rg,F}|_{up}^{n+1}\right]$, is a strongly non-linear function. The single-point upstream weighting technique is used to calculate this term.

$$if\ \Phi_{g,F}|_i^{n+1} \geq \Phi_{g,F}|_{i+1}^{n+1} \rightarrow k_{rg,F}|_{up}^{n+1} = k_{rg,F}|_i^{n+1}$$

$$if\ \Phi_{g,F}|_i^{n+1} < \Phi_{g,F}|_{i+1}^{n+1} \rightarrow k_{rg,F}|_{up}^{n+1} = k_{rg,F}|_{i+1}^{n+1} \tag{3.33}$$

The transmissibility terms for the diffusion flow is similar to the transmissibility term of Darcian flow above. Also take the terms from equation 3.27 as an example.

$$\left[\frac{D_F A_x}{5.615\Delta x}\Big|_{i+\frac{1}{2}}\right]\left[\phi_F S_{g,F}\Big|_{i+\frac{1}{2}}\right]$$

Since we assume the diffusion coefficient is a constant, the first term, $\left[\frac{D_F A_x}{\Delta x}\Big|_{i+\frac{1}{2}}\right]$, is a linear term related to the dimension of grid blocks only. Therefore, it could be calculated using harmonic average.

$$\left[\frac{D_F A_x}{5.615\Delta x}\Big|_{i+\frac{1}{2}}\right] = \frac{D_F}{5.615} \times \frac{2A_x|_i A_x|_{i+1}}{A_x|_i \Delta x|_{i+1} + A_x|_{i+1}\Delta x|_i} \tag{3.34}$$

The second term, $\left[\phi_F S_{g,F}\Big|_{i+\frac{1}{2}}\right]$, is also calculated by the harmonic average technique.

$$\left[\phi_F S_{g,F}\Big|_{i+\frac{1}{2}}\right] = \frac{2\phi_F S_{g,F}|_i \phi_F S_{g,F}|_{i+1}}{\phi_F S_{g,F}|_i + \phi_F S_{g,F}|_{i+1}} \tag{3.35}$$

The above terms were using gas equation as an example. The transmissibility terms for water phase could use the same procedure to calculate.

3.4 Source/Sink Terms

In this model, the source/sink terms can be categorized in three different groups. Firstly, the flow between the fracture and matrix domain could be treated as an implicit source term. Second, the flow inject or produce from the wellbore. Thirdly, the gas flow release from the matrix.

3.4.1 Flow between fracture and matrix domain

We also take the term from equation 3.27 as an example to represent the gas flow transfer between fracture and matrix system in a grid block. Chawathe et al. (1996) developed the

correlation that describes the transport phenomena of methane from matrix to fracture in fractured reservoirs.

For gas phase

$$\Gamma_{g,F}\big|_i^{n+1} = 5.615\sigma V_b|_i \left(\frac{T_{sc}}{TP_{sc}}\right)\left[\frac{k_{rg,up}\big|_i^{n+1}\overline{k_M}\big|_i^{n+1}}{\mu_g\left(\overline{P_g}\big|_i^{n+1}\right) z\left(\overline{P_g}\big|_i^{n+1}\right)}\right]\left[\frac{\left(P_{g,M}\big|_i^{n+1}\right)^2 - \left(P_{g,F}\big|_i^{n+1}\right)^2}{2}\right]$$

$$+ 5.615\sigma V_b|_i \left(\frac{T_{sc}}{TP_{sc}}\right) D_M \left[\frac{P_{g,M}\big|_i^{n+1} S_{g,M}\big|_i^{n+1}}{z\left(P_{g,M}\big|_i^{n+1}\right)} - \frac{P_{g,F}\big|_i^{n+1} S_{g,F}\big|_i^{n+1}}{z\left(P_{g,F}\big|_i^{n+1}\right)}\right] \tag{3.36}$$

$\overline{P_g}\big|_i^{n+1}$ is the arithmetic average of the gas pressure in fracture and matrix domain for a specific grid block. D_M is the diffusion coefficient in matrix since diffusion has dominant effect in matrix system. $\overline{k_M}\big|_i^{n+1}$ is the geometric average permeability from x, y, and z directions. σ is the shape factor, developed by Lim and Aziz (1995), which control the amount of the flow through matrix to fracture.

$$\sigma = \pi^2\left(\frac{1}{L_x^2} + \frac{1}{L_y^2} + \frac{1}{L_z^2}\right) \tag{3.37}$$

L_x, L_y, and L_z are the lengths of the coal matrix (fracture spacing) in x, y, and z directions, respectively. There are other options for the shape factors based on different boundary conditions.

Kazemi et al. (1976) $\qquad \sigma = 4\left(\frac{1}{L_x^2} + \frac{1}{L_y^2} + \frac{1}{L_z^2}\right)$ (3.38)

Coats (1989) $$\sigma = 8\left(\frac{1}{L_x^2}+\frac{1}{L_y^2}+\frac{1}{L_z^2}\right) \tag{3.39}$$

Chang (1993) $$\sigma = 12^2\left(\frac{1}{L_x^2}+\frac{1}{L_y^2}+\frac{1}{L_z^2}\right) \tag{3.40}$$

The gas relative permeability in equation 3.34 is also calculated using one-point upstream weighting method.

$$if\ \mathrm{P}_{g,M}\big|_i^{n+1} \geq \mathrm{P}_{g,F}\big|_i^{n+1} \rightarrow k_{rg,up}\big|_i^{n+1} = k_{rg,M}\big|_i^{n+1}$$

$$if\ \mathrm{P}_{g,M}\big|_i^{n+1} < \mathrm{P}_{g,F}\big|_i^{n+1} \rightarrow k_{rg,up}\big|_i^{n+1} = k_{rg,F}\big|_i^{n+1} \tag{3.38}$$

Here we used pressure (P) instead of potential gradient (Φ) is because here we only consider the flow between fracture and matrix in the same grid block. Therefore, there is no gravity difference between the fracture and matrix domain since they are at the same depth.

For water phase

$$\Gamma_{\mathrm{w,F}}\big|_i^{n+1} = \sigma V_b|_i \left[\frac{k_{rw,up}\big|_i^{n+1}\overline{k_M}|_i^{n+1}}{\mu_w(\overline{P_w}|_i^{n+1})B_w(\overline{P_w}|_i^{n+1}|)}\right]\left[\left(P_{w,M}\big|_i^{n+1}\right)-\left(P_{w,F}\big|_i^{n+1}\right)\right] \tag{3.39}$$

Similar to the calculation method of gas equations 3.36, $\overline{P_w}|_i^{n+1}$ is the arithmetic average of water pressure between fracture and matrix domain, and the water relative permeability is also calculated by one-point upstream weighting method.

$$if\ \mathrm{P}_{w,M}\big|_i^{n+1} \geq \mathrm{P}_{w,F}\big|_i^{n+1} \rightarrow k_{rw,up}\big|_i^{n+1} = k_{rw,M}\big|_i^{n+1}$$

$$if\ \mathrm{P}_{w,M}\big|_i^{n+1} < \mathrm{P}_{w,F}\big|_i^{n+1} \rightarrow k_{rw,up}\big|_i^{n+1} = k_{rw,F}\big|_i^{n+1} \tag{3.40}$$

3.4.2 Flow injected or produced from a wellbore

In this model, we use Peaceman's wellbore equation to calculate the flow rate at a wellbore.

For gas flow rate at wellbore

$$q_g\big|_i^{n+1} = -\frac{2\pi 5.615 T_{SC} P_{g,F}\big|_i^{n+1}}{T P_{SC}}\left[\frac{k_{rg,F}\big|_i^{n+1}\overline{k_F}\big|_i^{n+1} h_i\left(P_{g,F}\big|_i^{n+1} - P_{wf}\big|_i^{n+1}\right)}{\mu_g\left(P_{g,F}\big|_i^{n+1}\right) z\left(P_{g,F}\big|_i^{n+1}\right)\left[\ln\left(\frac{r_e|_i}{r_w|_i}\right) + s_i\right]}\right]$$

$$-\frac{2\pi 5.615 T_{SC}}{T P_{SC}} D_F h_i\left[\frac{\frac{P_{g,F}\big|_i^{n+1} S_g\big|_i^{n+1}}{z\left(P_{g,F}\big|_i^{n+1}\right)} - \frac{P_{wf}\big|_i^{n+1} S_g\big|_i^{n+1}}{z\left(P_{wf}\big|_i^{n+1}\right)}}{\left[\ln\left(\frac{r_e|_i}{r_w|_i}\right) + s_i\right]}\right] \tag{3.41}$$

For water flow rate at wellbore

$$q_w\big|_i^{n+1} = \frac{-2\pi k_{rw,F}\big|_i^{n+1}\overline{k_F}\big|_i^{n+1} h_i\left(P_{w,F}\big|_i^{n+1} - P_{wf}\big|_i^{n+1}\right)}{\mu_w\left(P_{w,F}\big|_i^{n+1}\right) B_w\left(P_{w,F}\big|_i^{n+1}\right)\left[\ln\left(\frac{r_e|_i}{r_w|_i}\right) + s_i\right]} \tag{3.42}$$

If we have vertical wells

$$r_e|_i = 0.28\left\{\frac{\left[\left(\frac{k_y}{k_x}\right)_i^{\frac{1}{2}}(\Delta x)_i^2 + \left(\frac{k_x}{k_y}\right)_i^{\frac{1}{2}}(\Delta y)_i^2\right]^{\frac{1}{2}}}{\left(\frac{k_y}{k_x}\right)_i^{\frac{1}{4}} + \left(\frac{k_x}{k_y}\right)_i^{\frac{1}{4}}}\right\}$$

$$\overline{k_F}\big|_i^{n+1} = \sqrt{k_x\, k_y}$$

In equation 3.39 and 3.40, the average permeability, $\overline{k_F}\big|_i^{n+1}$, is calculated using geometric average of the permeability perpendicular to wellbore direction, which means if we have a vertical well (z direction), the average permeability will be the geometric mean of the permeability in x and y directions.

3.4.3 Gas sorption term

Adsorbed gas is an physics need to be captured in CBM production simulation because majority (up to 98%) of gas in CBM reservoir is stored via the adsorbed state (Satya Harpalani 1984). Since we assume that the gas is only methane, the Langmuir adsorption model could be used here to calculate the amount of gas release from the matrix due to the reservoir pressure decrease when the well is producing.

$$V_E = \frac{V_L P}{P_L + P} \tag{3.43}$$

V_E is the pure component adsorption capacity at equilibrium condition, P is the reservoir pressure, V_L is the sorption volume constant, and P_L is the sorption pressure constant. In order to incorporate the gas sorption rate into the continuity equations, this term for each time step could be calculated as follow:

$$q_{srp}\big|_i^{n+1} = \frac{\rho_c V_b|_i (V_E|_i^{n+1} - V_E|_i^n)}{\Delta t} \tag{3.44}$$

3.5 Correlations for Rock and Fluid Properties

Gas Formation Volume Factor

$$B_g = \frac{P_{sc} z T}{5.615 P Z_{sc} (T_{SC} + 460)} \tag{3.45}$$

Gas Density

$$\rho_g = \frac{PM_g}{ZR(T+460)} \tag{3.46}$$

Gas Viscosity

$$\mu_g = 1 \times 10^{-4} k_v EXP\left(x_v \left(\frac{\rho_g}{62.4}\right)^{y_v}\right) \tag{3.47}$$

Where

$$k_v = \frac{(9.4 + 0.02M_g)T^{1.5}}{209 + 19M_g + T}$$

$$y_v = 2.4 - 0.2x_v$$

$$x_v = 3.5 + \frac{986}{T} + 0.01M_g$$

Relative Permeability to Gas

Corey's correlation:

$$k_{rg} = k_{rgc}(1 - S_{wn}^2)(1 - S_{wn})^2 \tag{3.48}$$

where

$$k_{rgc} = k_{rg}\ at\ S_g = 1 - S_{wirr}$$

$$S_{wn} = \frac{S_w - S_{wirr}}{1 - S_{girr} - S_{wirr}}$$

Relative Permeability to Water

Corey's correlation:

$$k_{rw} = k_{rwc} S_{wn}^4 \tag{3.49}$$

where

$$k_{rwc} = k_{rw}\ at\ S_w = 1 - S_{girr}$$

$$S_{wn} = \frac{S_w - S_{wirr}}{1 - S_{girr} - S_{wirr}}$$

Capillary Pressure

Corey's correlation:

$$P_{cgw} = \frac{1}{\sqrt{1.448(S_w - S_{wirr})}} \tag{3.50}$$

Water Properties

Table 3 Water properties used in the model

Pressure (psia)	ρ_w (lb/ft^3)	B_w (RB/STB)	μ_w (cP)	R_{sw} (SCF/STB)
14.7	62.24	1.041	0.31	0
270	62.28	1.0403	0.31	0
520	62.33	1.0395	0.31	0
1015	62.42	1.038	0.31	0
2015	62.6	1.035	0.31	0
2512	62.69	1.0335	0.31	0
3015	62.78	1.032	0.31	0
4015	62.96	1.029	0.31	0
5015	63.16	1.0258	0.31	0
9015	63.96	1.013	0.31	0

3.6 Generalized Newton-Raphson Procedure

The numerical model now has 8 non-linear equations due to the equations are strongly functions of the dependent variables (gas pressure and saturation in fracture & matrix). Since analytical solutions in such cases are impossible to obtain, the generalized Newton-Raphson procedure is used to linearize all the non-linear equations and produce a set of linear equations. By using the auxiliary equations in section 3.2 into the residual form of governing equations in

section 3.3, we will then have only 4 primary unknowns instead of 8 in each grid block. The linearized residual form equations for each phase in each domain are listed as follow (in 1-D form):

Gas phase in fracture domain

$$R_{g,F}\Big|^{n+1}\Big|^{k} = -\left\{\frac{\partial R_{g,F}}{\partial P_{g,F}}\Big|^{n+1}\Big|^{k} \Delta P_{g,F}\Big|^{n+1}\Big|^{k+1} + \frac{\partial R_{g,F}}{\partial P_{g,M}}\Big|^{n+1}\Big|^{k} \Delta P_{g,M}\Big|^{n+1}\Big|^{k+1} + \frac{\partial R_{g,F}}{\partial S_{g,F}}\Big|^{n+1}\Big|^{k} \Delta S_{g,F}\Big|^{n+1}\Big|^{k+1} + \frac{\partial R_{g,F}}{\partial S_{g,M}}\Big|^{n+1}\Big|^{k} \Delta S_{g,M}\Big|^{n+1}\Big|^{k+1}\right\} \tag{3.51}$$

Water phase in fracture domain

$$R_{w,F}\Big|^{n+1}\Big|^{k} = -\left\{\frac{\partial R_{w,F}}{\partial P_{g,F}}\Big|^{n+1}\Big|^{k} \Delta P_{g,F}\Big|^{n+1}\Big|^{k+1} + \frac{\partial R_{w,F}}{\partial P_{g,M}}\Big|^{n+1}\Big|^{k} \Delta P_{g,M}\Big|^{n+1}\Big|^{k+1} + \frac{\partial R_{w,F}}{\partial S_{g,F}}\Big|^{n+1}\Big|^{k} \Delta S_{g,F}\Big|^{n+1}\Big|^{k+1} + \frac{\partial R_{w,F}}{\partial S_{g,M}}\Big|^{n+1}\Big|^{k} \Delta S_{g,M}\Big|^{n+1}\Big|^{k+1}\right\} \tag{3.52}$$

Gas phase in matrix domain

$$R_{g,M}\Big|^{n+1}\Big|^{k} = -\left\{\frac{\partial R_{g,M}}{\partial P_{g,F}}\Big|^{n+1}\Big|^{k} \Delta P_{g,F}\Big|^{n+1}\Big|^{k+1} + \frac{\partial R_{g,M}}{\partial P_{g,M}}\Big|^{n+1}\Big|^{k} \Delta P_{g,M}\Big|^{n+1}\Big|^{k+1} + \frac{\partial R_{g,M}}{\partial S_{g,F}}\Big|^{n+1}\Big|^{k} \Delta S_{g,F}\Big|^{n+1}\Big|^{k+1} + \frac{\partial R_{g,M}}{\partial S_{g,M}}\Big|^{n+1}\Big|^{k} \Delta S_{g,M}\Big|^{n+1}\Big|^{k+1}\right\}$$

(3.53)

Water phase in matrix domain

$$R_{w,M}\Big|^{n+1}\Big|^{k} = -\left\{\frac{\partial R_{w,M}}{\partial P_{g,F}}\Big|^{n+1}\Big|^{k} \Delta P_{g,F}\Big|^{n+1}\Big|^{k+1} + \frac{\partial R_{w,M}}{\partial P_{g,M}}\Big|^{n+1}\Big|^{k} \Delta P_{g,M}\Big|^{n+1}\Big|^{k+1}\right.$$
$$\left. + \frac{\partial R_{w,M}}{\partial S_{g,F}}\Big|^{n+1}\Big|^{k} \Delta S_{g,F}\Big|^{n+1}\Big|^{k+1} + \frac{\partial R_{w,M}}{\partial S_{g,M}}\Big|^{n+1}\Big|^{k} \Delta S_{g,M}\Big|^{n+1}\Big|^{k+1}\right\}$$

(3.54)

The above four linear equations, which including two fracture network equations and two coal matrix equations, could then be solved by an iterative protocol to simultaneously get four solutions ($P_{g,F}$, $P_{g,M}$, $S_{g,F}$, $S_{g,M}$). The superscripts k+1 in the iteration process indicates the current iteration level while k represents the previous iteration level. Combined the above four equations, we could have a matrix form of those equations to illustrate how the unknowns been solved in our numerical model.

$$\begin{bmatrix} \frac{\partial R_{g,F}}{\partial P_{g,F}} & \frac{\partial R_{g,F}}{\partial P_{g,M}} & \frac{\partial R_{g,F}}{\partial S_{g,F}} & \frac{\partial R_{g,F}}{\partial S_{g,M}} \\ \frac{\partial R_{w,F}}{\partial P_{g,F}} & \frac{\partial R_{w,F}}{\partial P_{g,M}} & \frac{\partial R_{w,F}}{\partial S_{g,F}} & \frac{\partial R_{w,F}}{\partial S_{g,M}} \\ \frac{\partial R_{g,M}}{\partial P_{g,F}} & \frac{\partial R_{g,M}}{\partial P_{g,M}} & \frac{\partial R_{g,M}}{\partial S_{g,F}} & \frac{\partial R_{g,M}}{\partial S_{g,M}} \\ \frac{\partial R_{w,M}}{\partial P_{g,F}} & \frac{\partial R_{w,M}}{\partial P_{g,M}} & \frac{\partial R_{w,M}}{\partial S_{g,F}} & \frac{\partial R_{w,M}}{\partial S_{g,M}} \end{bmatrix}^{k} \begin{bmatrix} \Delta P_{g,F} \\ \Delta P_{g,M} \\ \Delta S_{g,F} \\ \Delta S_{g,M} \end{bmatrix}^{k+1} = -\begin{bmatrix} R_{g,F} \\ R_{g,M} \\ R_{w,F} \\ R_{w,M} \end{bmatrix}^{k}$$

3.7 Permeability Evolution Module

As mentioned in chapter 2, in coalbed methane production process, permeability evolution is a well-accepted phenomenon, which consist of two parts: 1. Permeability decrease due to the

effective stress increase during production. 2. Permeability increase since the matrix shrinkage due to stored gas coming out from the matrix to the fracture. In our model, we had incorporated different permeability evolution model which were based on different assumption and condition. Palmer and Mansoori (1996) proposed a strain-based model which is derived from the cubic relationship between permeability and porosity and the equation of elasticity for strain in porous rock. The P&M model could be expressed as follow:

$$\frac{k}{k_i} = \left(\frac{\phi}{\phi_i}\right)^3 = \left[1 + \frac{\widetilde{C_m}}{\phi_i}(p - p_i) + \frac{\varepsilon_l}{\phi_i}\left[\frac{K}{M} - 1\right]\left(\frac{p}{p_L+p} - \frac{p_i}{p_L+p_i}\right)\right]^3 \tag{3.55}$$

where $\widetilde{C_m} = \frac{1}{M} - \left[\frac{K}{M} + f - 1\right]\gamma$

Shi and Durucan (2005) proposed another stress-based model derived from the exponential relationship between the ratio of permeability and the change in effective stress. The volumetric-shrinkage strain is related to the amount of gas desorbed from the matrix. The S&D model could be written as follow:

$$\frac{k}{k_i} = exp\left\{-3C_f\left[-\frac{v}{1-v}(p - p_i) + \frac{E\alpha_s V_L}{3(1-v)}\left(\frac{p}{p_L+p} - \frac{p_i}{p_L+p_i}\right)\right]\right\} \tag{3.56}$$

The above two models (P&M and S&D) did not account for the effects of water in the coal matrix on the gas sorption. Therefore, (Thararoop, Karpyn, and Ertekin 2009) developed a model incorporated such effect into coal shrinkage and swelling behavior, which is the parameter $\tilde{f}$ called sorption capacity factor. The equation is as follow:

$$\frac{k}{k_i} = \left[e^{C_p(p-p_i)} + \frac{\tilde{f}\beta\rho V_m}{\phi_i}\left(\frac{p_i}{p_L+p_i} - \frac{p}{p_L+p}\right)\right]^3 \tag{3.57}$$

where $C_p = \frac{1}{2E\phi_i}$

S. Liu and Harpalani (2013) presented a new theoretical model for the sorption-induced volumetric strain and coupled to the P&M and S&D models. They believed the desorption-induced matrix shrinkage could not analogous with thermal shrinkage as in P&M and S&D model. Therefore, the coupled forms are as follow:

$$\frac{k}{k_i} = \left(\frac{\phi}{\phi_i}\right)^3 = \left[1 + \frac{\widetilde{C_m}}{\phi_i}(p - p_i) + \frac{1}{\phi_i}\left[\frac{K}{M} - 1\right]\Delta\varepsilon\right]^3 \tag{3.58}$$

$$\frac{k}{k_i} = exp\left\{-3C_f\left[-\frac{v}{1-v}(p - p_i) + \frac{E}{3(1-v)}\Delta\varepsilon\right]\right\} \tag{3.59}$$

where $\Delta\varepsilon = \frac{3V_L\rho RT}{\mathrm{E_A V_o}}\int_{p_1}^{p_2}\frac{1}{P_L+P}dP$

We have coupled all five permeability evolution models in to our proposed model to compare the difference and perform the analysis.

Chapter 4 Model Validation

In this chapter, the proposed CBM model was tested and validated against a commercial reservoir simulator. The proposed CBM model will validated with single-porosity, single-permeability model, dual-porosity, single-permeability model, and dual-porosity, single-permeability with desorption mechanism.

4.1 Validation against the Single-porosity, Single-permeability Model (Case 1 and Case 2)

The dual-porosity, dual permeability CBM reservoir model was first simplified to simulate flow in a single-porosity, single permeability reservoir and being validated against a commercial software.

In order to use our model to simulate the flow in single-porosity, single permeability reservoir, the fracture porosity and matrix permeability are set close to zero, which simplifies our model to a single-porosity, single-permeability one. Case 1 and 2 are done for validation with single phase flow and two-phase flow production, respectively. Table 4 and Figure 8 are the input data for validation case 1.

Table 4 Input data for validation case 1

Parameters	Single-ϕ single-k	Dual-ϕ dual-k	units
Reservoir size	1100x1100	1100x1100	ft
Reservoir thickness	10	10	ft
Fracture porosity	8	0.0000001	%
Matrix porosity	-	8	%
Fracture permeability	80	80	md
Matrix permeability	-	0.00001	md
Initial pressure	1100	1100	psia
Fracture spacing	-	0.01	ft
Initial water saturation, fracture	15	15	%
Initial water saturation, matrix	-	15	%
Irreducible water saturation	20	20	%
Reservoir temperature	80	80	°F
Number of grid blocks	11,11,1	11,11,1	-
Well location	6,6,1	6,6,1	-
Well radius	0.25	0.25	ft
Sandface pressure	14.7	14.7	psia
Skin factor	0	0	-

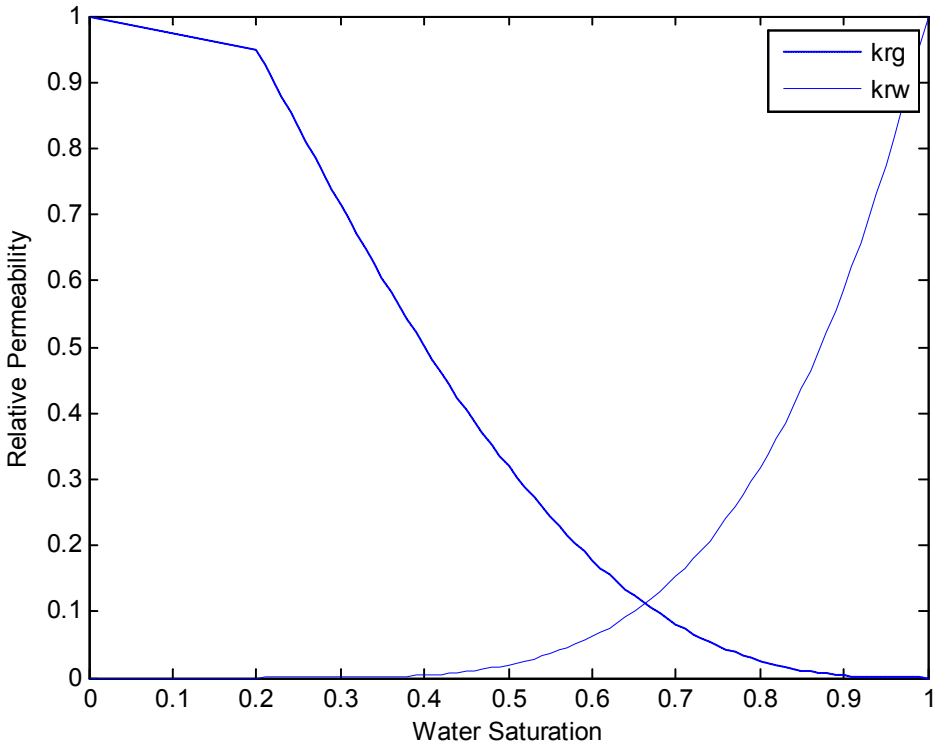

Figure 8 Water and gas relative permeability for validation test

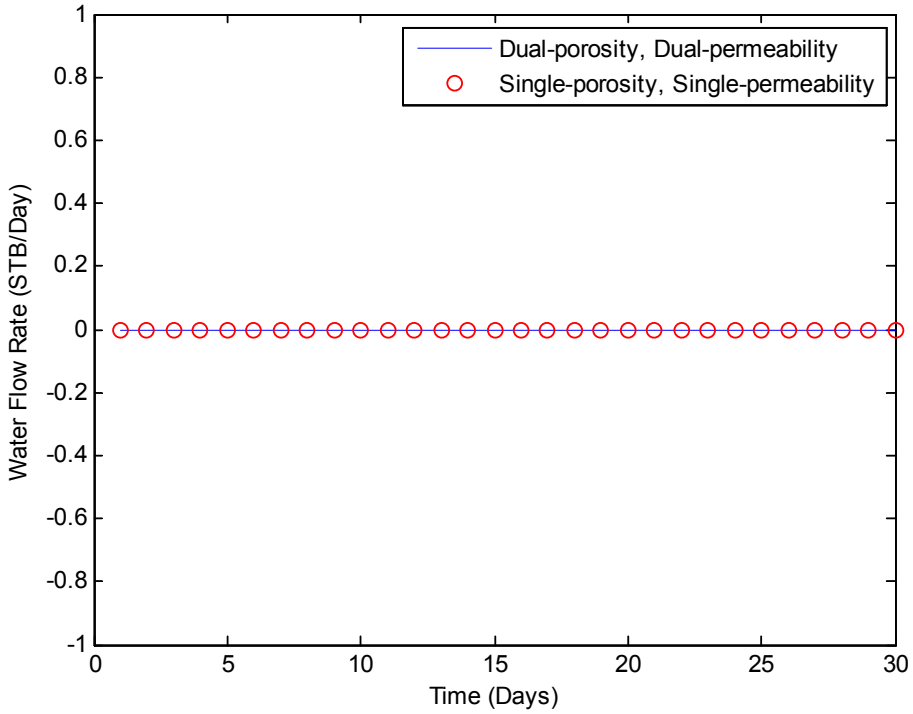

Figure 9 Water production profile for validation case 1

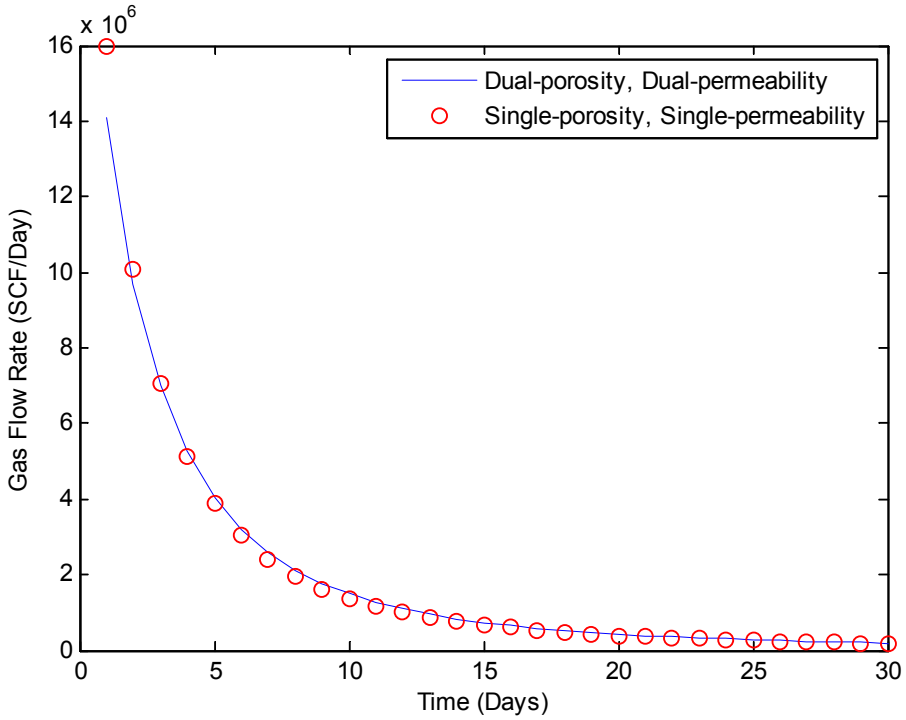

Figure 10 Gas production profile from validation case 1

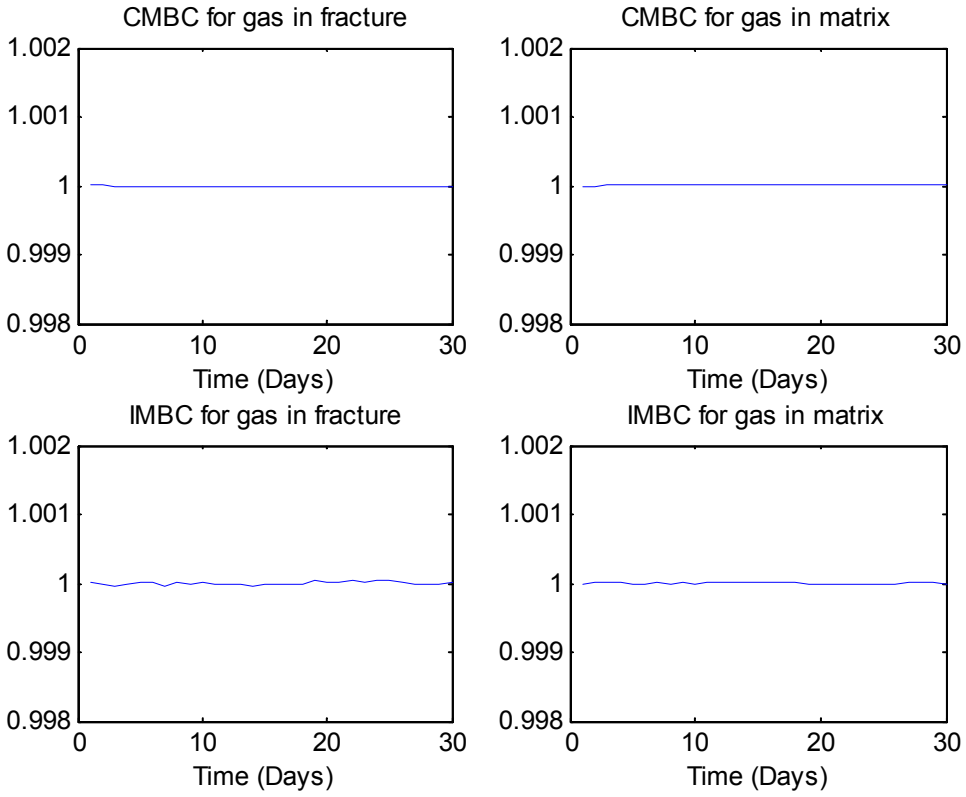

Figure 11 Material balance check for gas in both fracture and matrix domain (case 1)

Figure 9 shows the water production profile for case 1. Since the initial water saturation is lower than the irreducible water saturation, the water phase in the system is immobile. Therefore, there is no water production in this case 1. Figure 10 shows the gas production results for case 1. It can be observed that the predicted gas production from these two models are in good agreement. Also, the material balance check (IMBC and CMBC) at each time step for gas in both fracture and matrix domain are less than the criteria which is 10^{-3} (Figure 11).

In validation case 2, the input parameters are similar to validation case 1. The difference is initial water saturation had been changed to a higher number than the irreducible water saturation, which will make the producing fluid became two phase flow in the systems.

Table 5 Input data for validation case 2

Parameters	Single-ϕ single-k	Dual-ϕ dual-k	units
Reservoir size	1100x1100	1100x1100	ft
Reservoir thickness	10	10	ft
Fracture porosity	8	0.0000001	%
Matrix porosity	-	8	%
Fracture permeability	80	80	md
Matrix permeability	-	0.00001	md
Initial pressure	1100	1100	psia
Fracture spacing	-	0.01	ft
Initial water saturation, fracture	40	40	%
Initial water saturation, matrix	-	40	%
Irreducible water saturation	20	20	%
Reservoir temperature	80	80	°F
Number of grid blocks	11,11,1	11,11,1	-
Well location	6,6,1	6,6,1	-
Well radius	0.25	0.25	ft
Sandface pressure	14.7	14.7	psia
Skin factor	0	0	-

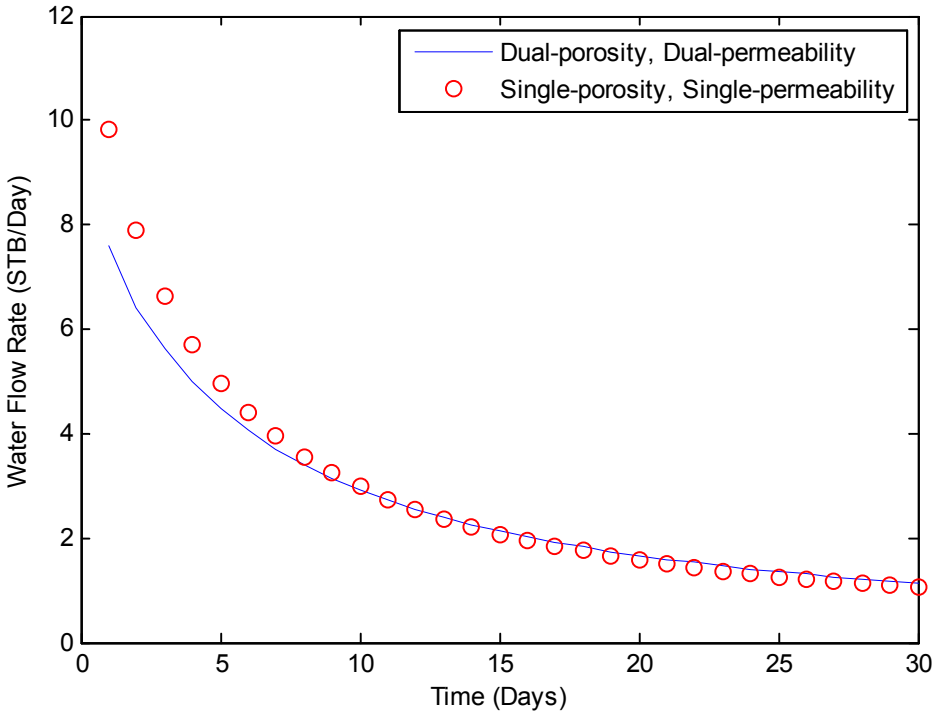

Figure 12 Water production profile for validation case 2

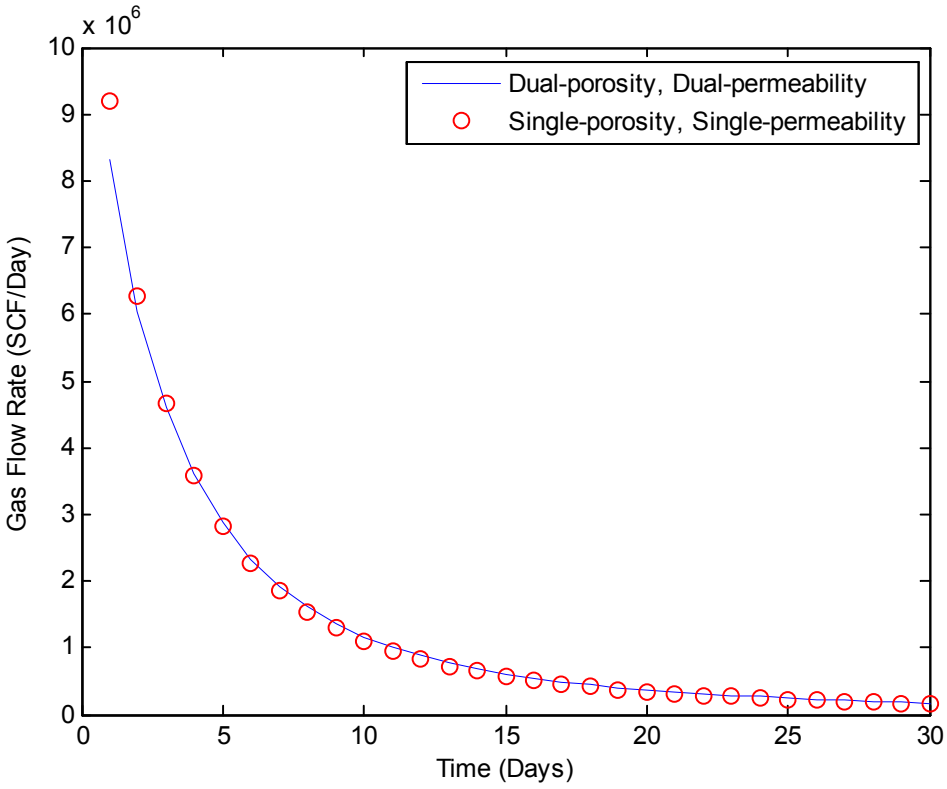

Figure 13 Gas production profile from validation case 2

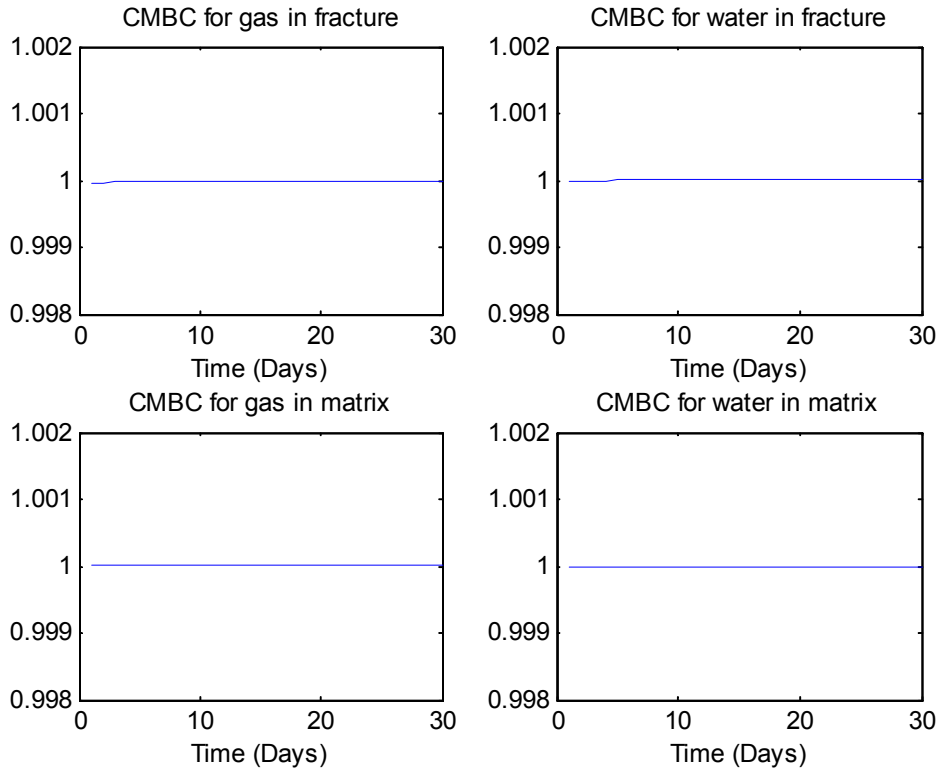

Figure 14 CMBC for gas and water in both matrix and fracture domain (case 2)

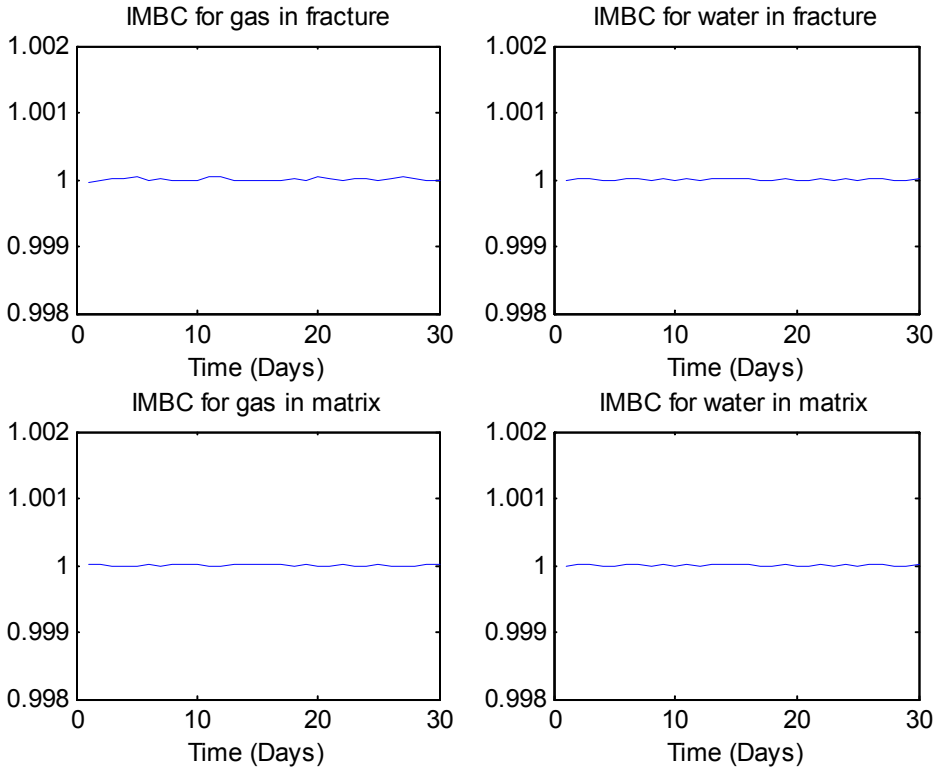

Figure 15 IMBC for gas and water in both matrix and fracture domain (case 2)

Figure 12 and Figure 13 show water production profile and gas production profile, respectively. It can also be observed that the predicted water and gas production from these two models are in good agreement. In addition, the material balance check (IMBC and CMBC) in each time step for gas and water in fracture and matrix domain are both less than the criteria which is 10^{-3}. The results of validation case 1 and case 2 conclude that the model is capable to simulate a single-porosity, single-permeability reservoir.

4.2 Validation against the Dual-Porosity, Single-Permeability Model (Case 3)

In validation case 3, the model was tested against the dual-porosity, single-permeability model in commercial software. The concept of dual-porosity, single permeability indicates that the matrix system is providing storage purpose and behave like a source/sink term for the fracture domain. Therefore, the fracture domain is the only field where fluid flows. Due to this

behavior, we assumed a very small value for the permeability in the matrix system, which can collapse the proposed CBM model to a dual-porosity, single permeability model. The reservoir system and input data for the validation case 3 are described in Table 6 and Figure 8

Table 6 Input data for validation case 3

Parameters	Dual-ϕ single-k	Dual-ϕ dual-k	units
Reservoir size	1100x1100	1100x1100	ft
Reservoir thickness	10	10	ft
Fracture porosity	0.0000001	0.0000001	%
Matrix porosity	8	8	%
Fracture permeability	80	80	md
Matrix permeability	0.00001	0.00001	md
Initial pressure	1100	1100	psia
Fracture spacing	0.01	0.01	ft
Initial water saturation, fracture	100	100	%
Initial water saturation, matrix	95	95	%
Irreducible water saturation	20	20	%
Reservoir temperature	80	80	°F
Number of grid blocks	11,11,1	11,11,1	-
Well location	6,6,1	6,6,1	-
Well radius	0.25	0.25	ft
Sandface pressure	14.7	14.7	psia
Skin factor	0	0	-
Coal density	1.435	1.435	g/cm

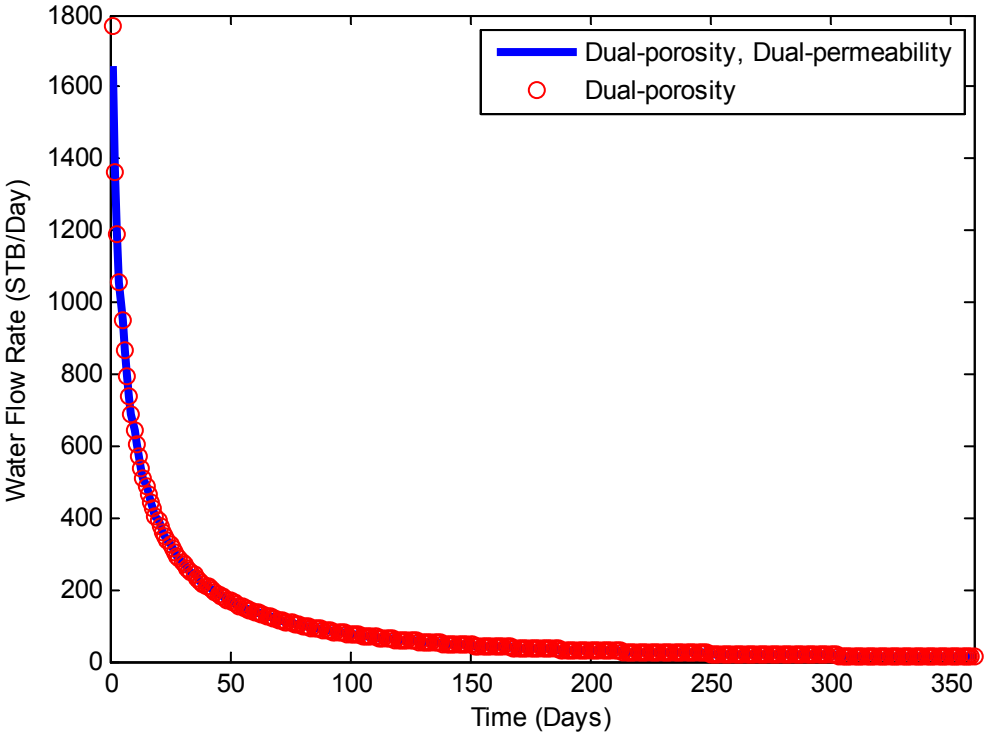

Figure 16 Water production profile for validation case 3

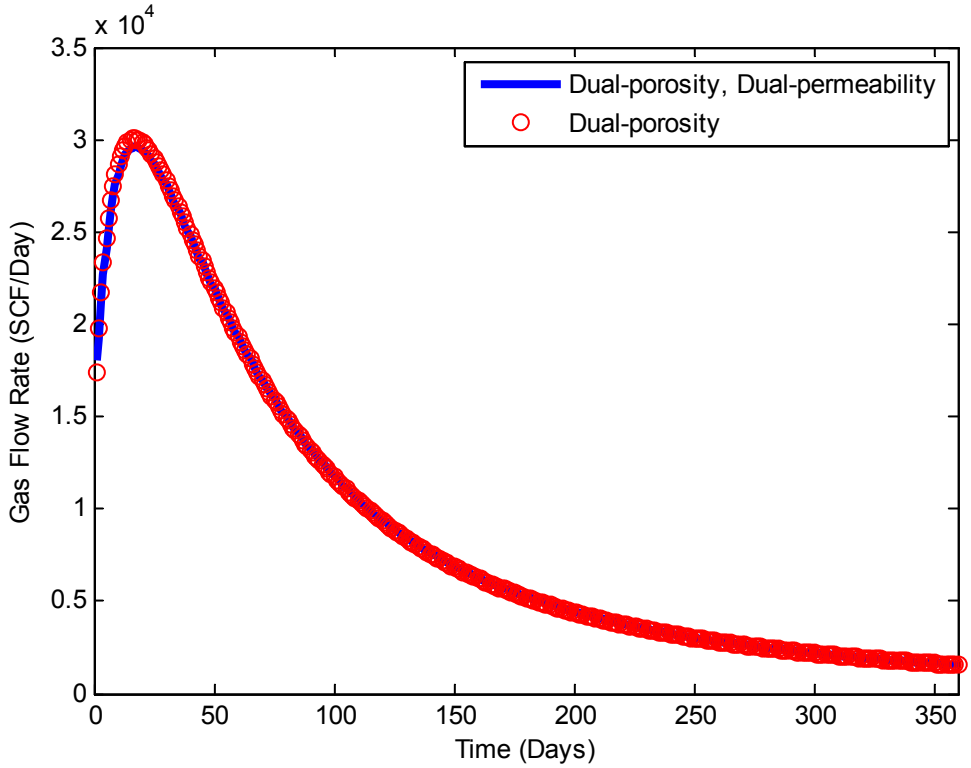

Figure 17 Gas production profile for validation case 3

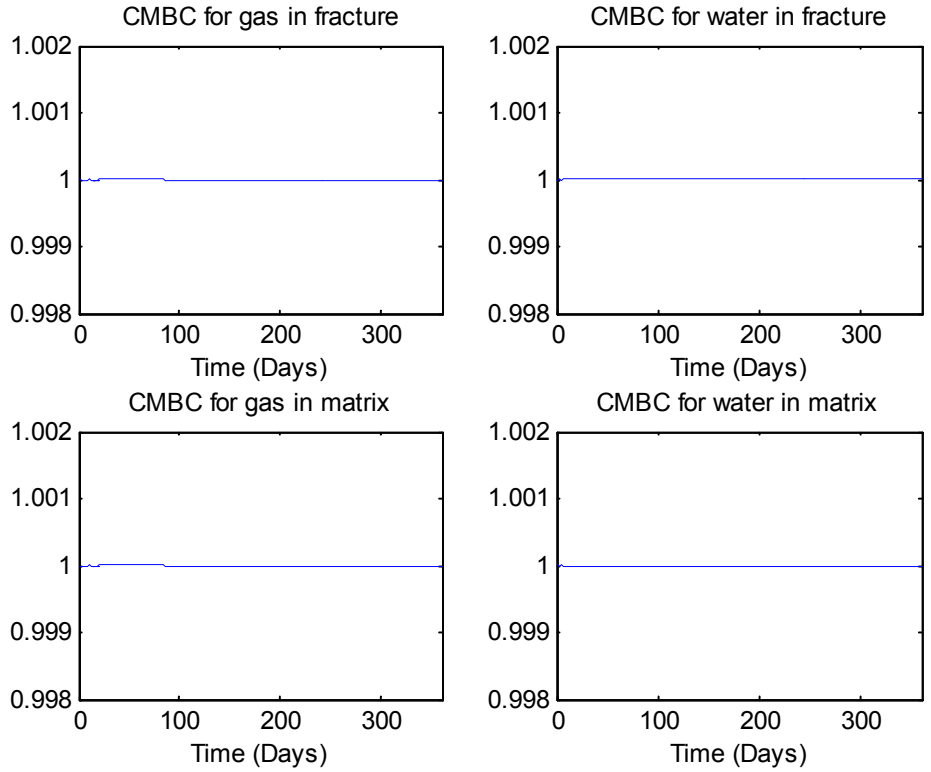

Figure 18 CMBC for gas and water in both matrix and fracture domain (case 3)

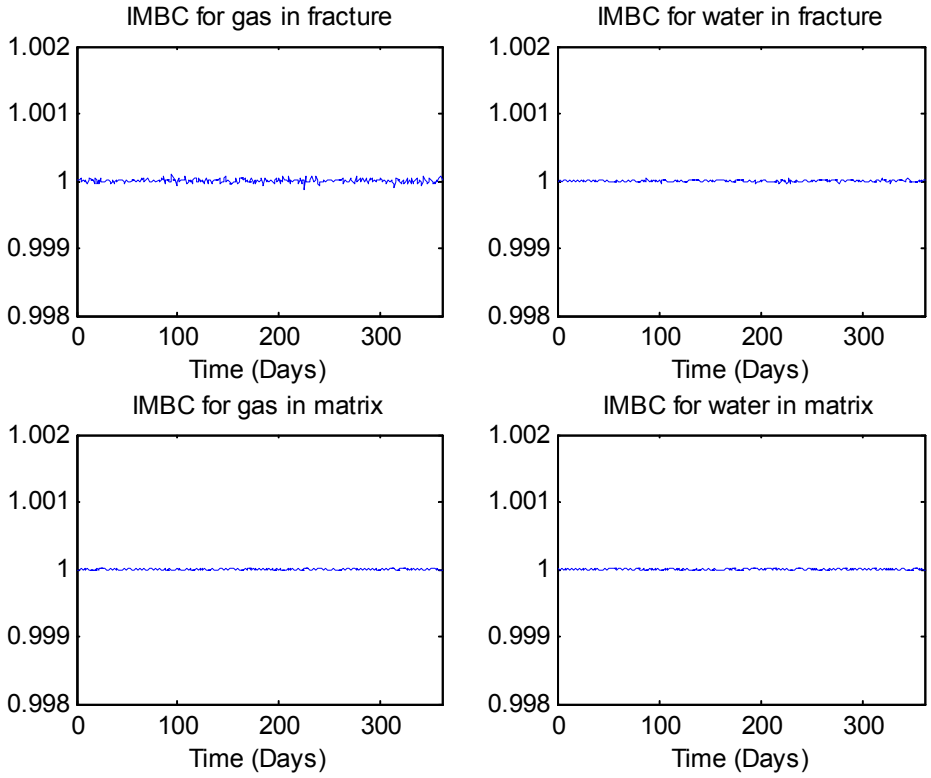

Figure 19 IMBC for gas and water in both matrix and fracture domain (case 3)

Figure 16 and Figure 17 show the predicted water and gas flow rate profile from two models, respectively. It can be observed that both gas flow rate and water flow rate from two models are in good agreement. Besides, the material balance check (IMBC and CMBC) for gas and water in both fracture and matrix domain is less than the criteria (Figure 18 and Figure 19). Therefore, the results from this case demonstrated that the model have the ability to simulate dual-porosity, single permeability reservoirs.

4.3 Validation for the Dual-porosity, Dual-permeability Model with Desorption (Case 4)

Since CBM reservoir is a naturally fractured systems with matrix and fracture domain and desorption is the major storage part for those reservoirs, we also did the validation case 4 for the desorption mechanism.

Table 7 Input data for validation case 4

Parameters	Dual-ϕ single-k	Dual-ϕ dual-k	units
Reservoir size	1100x1100	1100x1100	ft
Reservoir thickness	10	10	ft
Fracture porosity	1	1	%
Matrix porosity	5	5	%
Fracture permeability	40	40	md
Matrix permeability	0.08	0.08	md
Initial pressure	1630	1630	psia
Fracture spacing	0.5	0.5	ft
Initial water saturation, fracture	95	95	%
Initial water saturation, matrix	10	10	%
Irreducible water saturation	20	20	%
Reservoir temperature	114	114	°F
Number of grid blocks	11,11,1	11,11,1	-
Well location	6,6,1	6,6,1	-
Well radius	0.25	0.25	ft
Sandface pressure	14.7	14.7	psia

Skin factor	0	0	-
Coal density	1.435	1.435	g/cm
Langmuir volume	386.695	386.695	SCF/ton
Langmuir pressure	956.023	956.023	psia

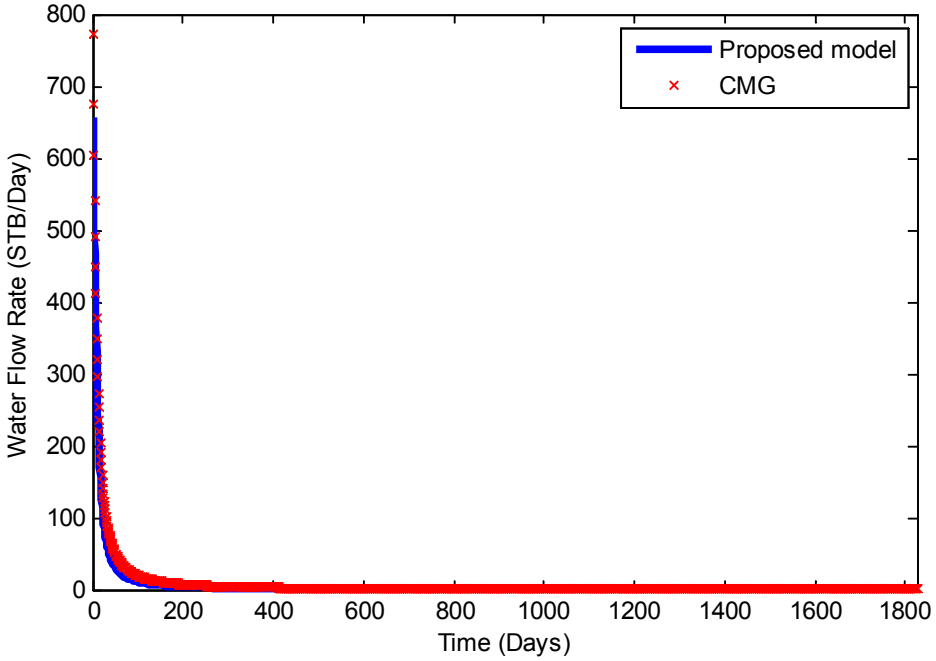

Figure 20 Water production profile for validation case 4

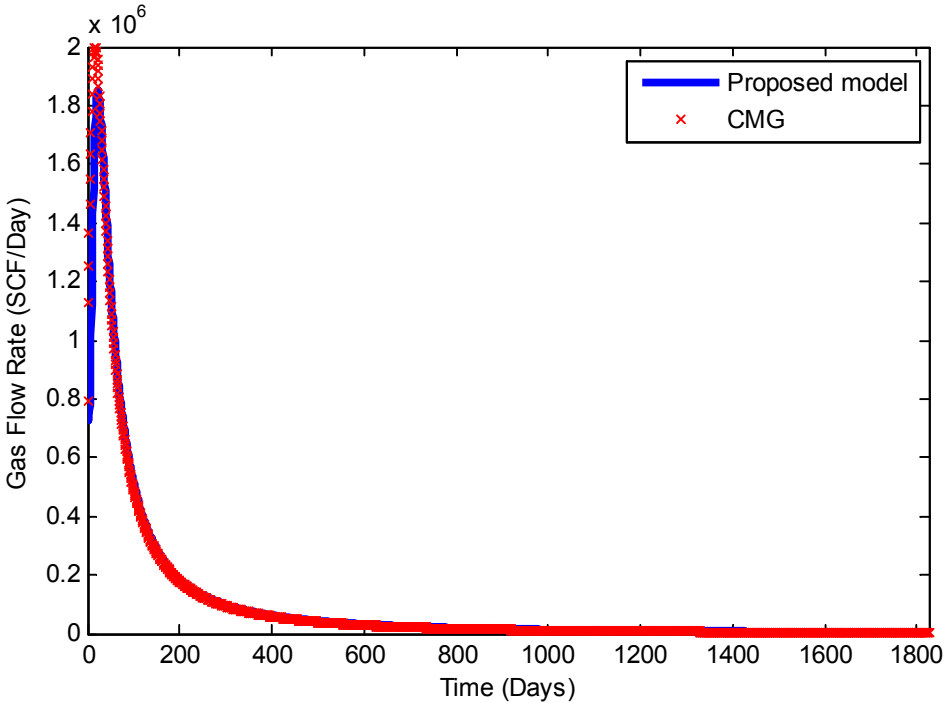

Figure 21 Gas production profile for validation case 4

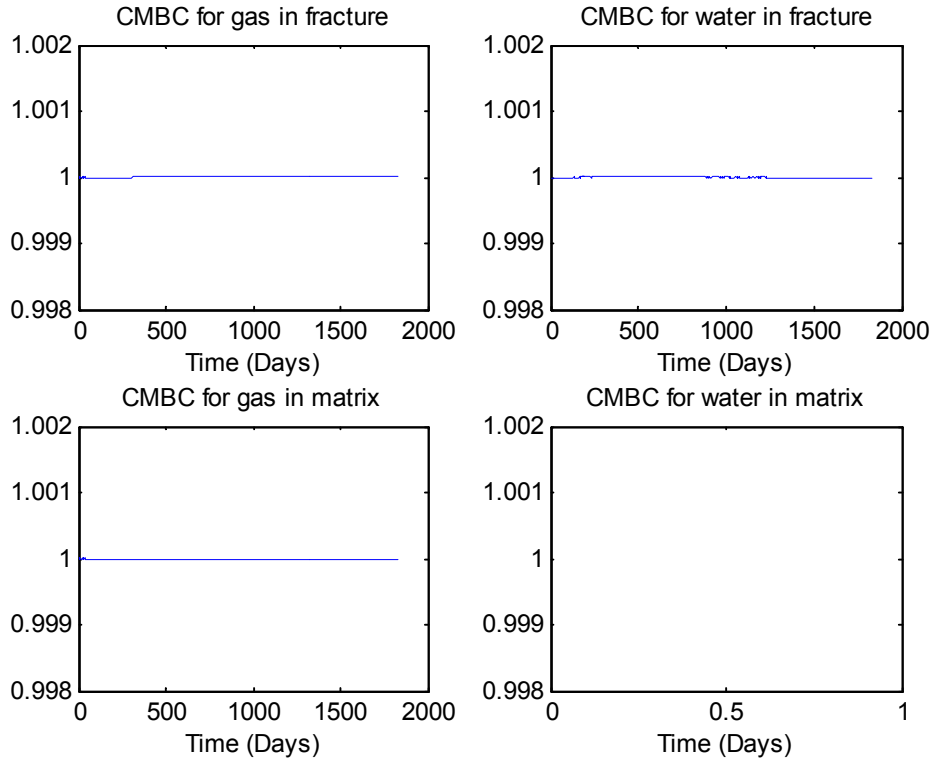

Figure 22 CMBC for gas and water in both matrix and fracture domain (case 4)

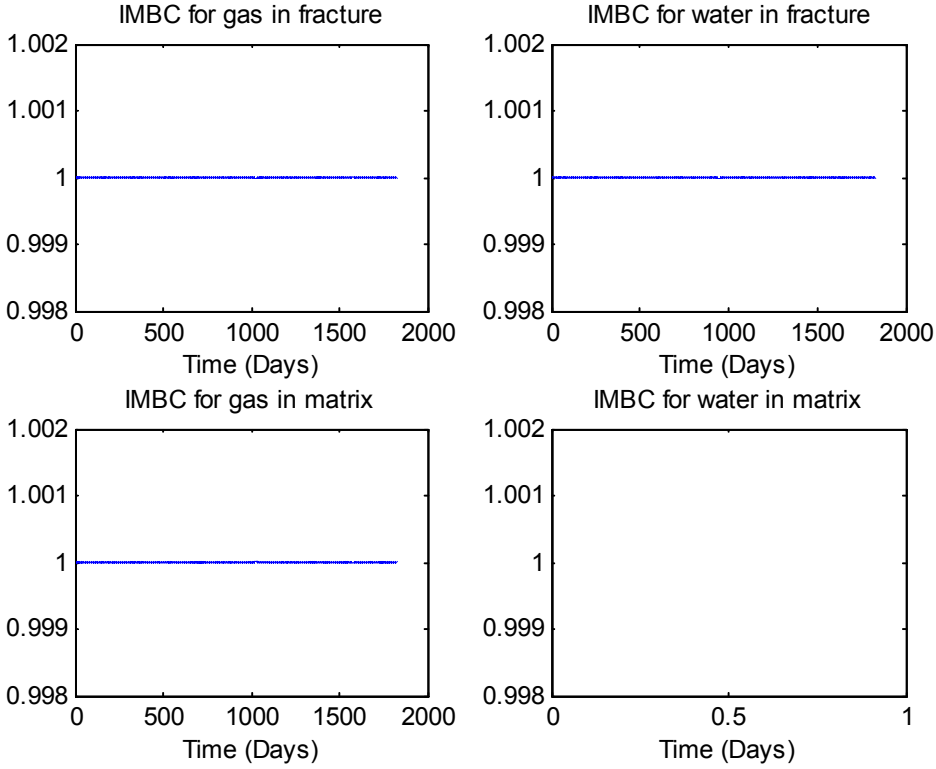

Figure 23 IMBC for gas and water in both matrix and fracture domain (case 4)

Figure 20 and Figure 21 are the simulation result predicting water flow rate and gas flow rate, respectively. The results show that both water and gas profile from two models are in good match. In addition, the material balance check (CMBC and IMBC) for gas and water in both fracture and matrix domain is less than the criteria (Figure 22 and Figure 23). Therefore, this validation case demonstrated the capability of the proposed model to simulate CBM reservoir coupled with desorption mechanism.

Chapter 5 Result and Analysis

In this chapter, we first run for a base case and then use the proposed model to perform a series of parametrical study to compare with the base case in order to see how those factors affect the production results, which including the effect of desorption, adsorption capacity, multi-mechanistic gas flow, cleat spacing, initial gas content, permeability evolution, dewatering operation, and hydraulic fracturing treatments.

5.1 Base case

In order to conduct the parametrical studies, we need to have a base case which contain all the mechanism and physics captured by the model. All the data were collected from the literatures based on CBM in San Juan Basin in USA. Table 8 are the parameters we used to run the base case.

Table 8 Input value for parameters in base case

Parameters	Dual-ϕ dual-k	units
Reservoir size	1100x1100	ft
Reservoir thickness	20	ft
Fracture porosity	0.1	%
Matrix porosity	0.5	%
Fracture permeability	5	md
Matrix permeability	0.005	md
Initial pressure	1100	psia
Fracture spacing	0.01	ft
Initial water saturation, fracture	100	%
Initial water saturation, matrix	95	%
Irreducible water saturation	20	%
Reservoir temperature	100	°F
Number of grid blocks	11,11,1	-
Well location	6,6,1	-
Well radius	0.25	ft

Sandface pressure	100	psia
Skin factor	0	-
Coal density	1.435	g/cm
Langmuir volume	906	SCF/ton
Langmuir pressure	625	psia
Initial gas content	100	%
Diffusion coefficient	1e-7	ft/Day

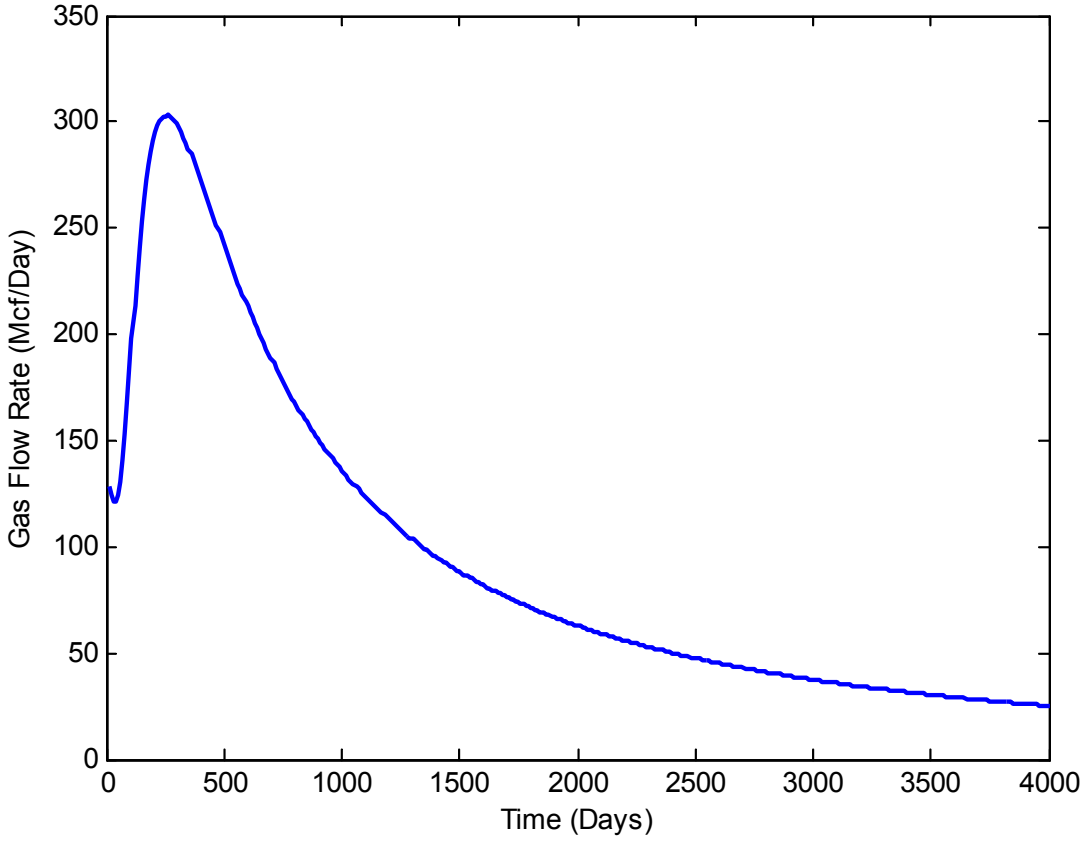

Figure 24 Gas production rate for base case

Figure 24 shows the gas flow rate versus time for the base case. The peak rate is around 300 Mcf/Day after 260 days of production period. The drainage area is about 28 acres in this case and the gas production rate is around 25 Mcf/Day after 4000 days production.

5.2 Effect of desorption

As mentioned in the chapter 2, adsorption is the major portion of gas storage in CBM reservoir. Parameters in Table 8 except Langmuir volume and pressure will be used to run a case without desorption.

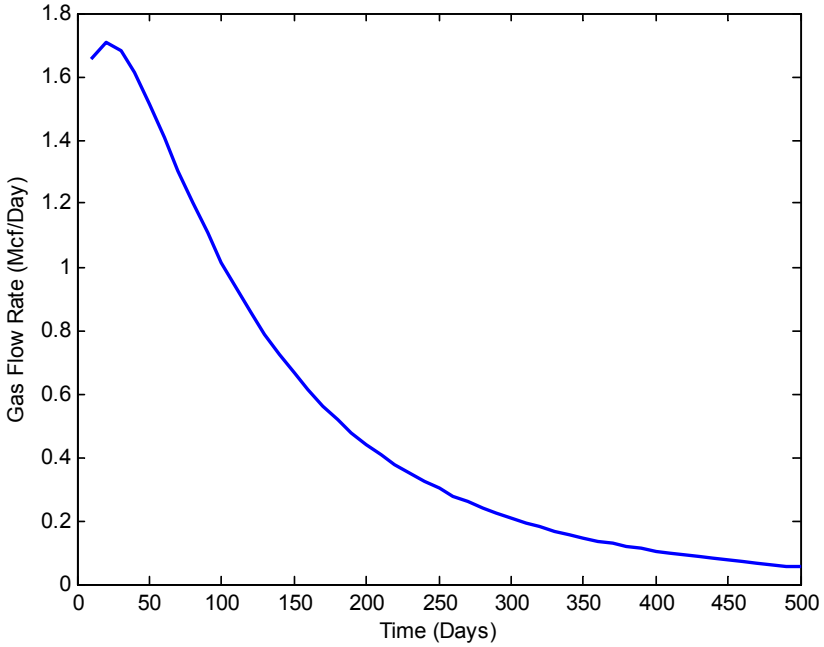

Figure 25 gas production rate for the case without desorption

Figure 25 is the gas production rate for the case without desorption. From the result at section 5.1, maximum production rate is 300 Mcf/Day at around 300 days. However, we could observe from Figure 25 that without desorption we will not have negative decline effect and the maximum gas rate is about 1.7 Mcf/Day at around 20 Days. There reason is that desorption gas acts like an additional source for production which will increase the original gas amount in the reservoir and results in a larger production rate. In addition, since the saturation of water is 100% in fracture domain and 95% in matrix domain, it shows at the very early time with a slight increase for the production rate then acts like a conventional reservoir. Therefore, peak flow rate with desorption is 177 times of that without desorption.

5.3 Effect of adsorption capacity

Different coal could have different adsorption capacity (also referred as Langmuir Volume constant). A higher rank coal has a curve that has an initially steep slope but levels out fast and maintain flat at high pressure. On the other hand, lower rank coals have a flatter curve throughout all pressures. We still used the data from the base case (Table 8) but tried it with different Langmuir Volume constant (1200, 906, 600 scf/ton) to see the effect of adsorption capacity.

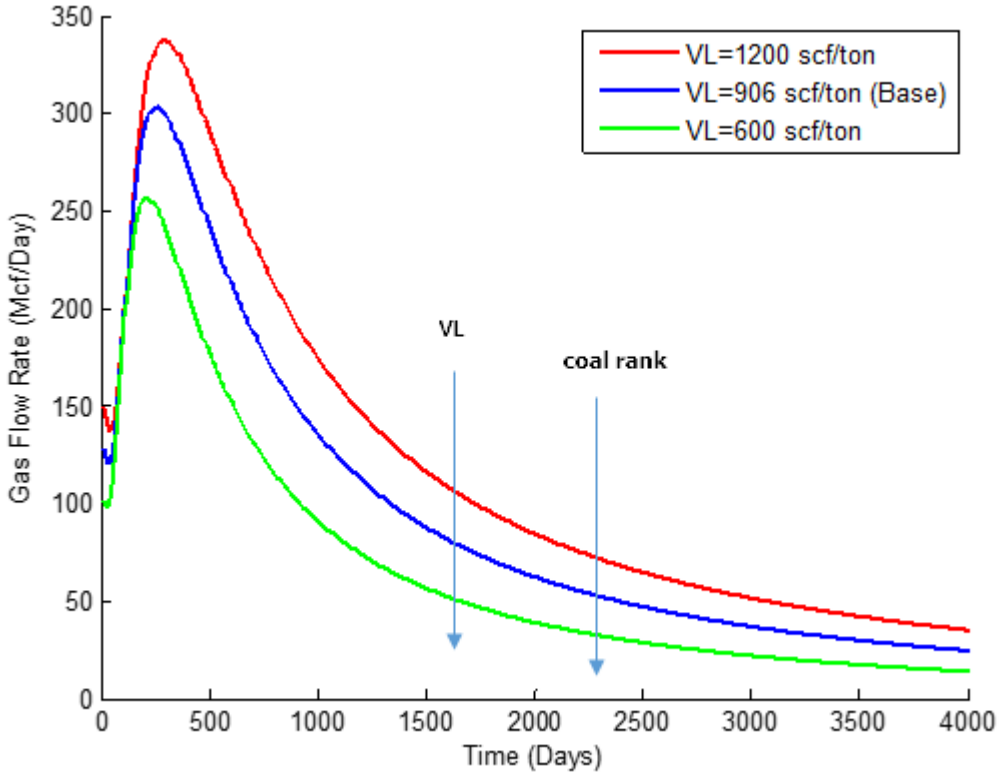

Figure 26 Gas rate profile for different adsorption capacity

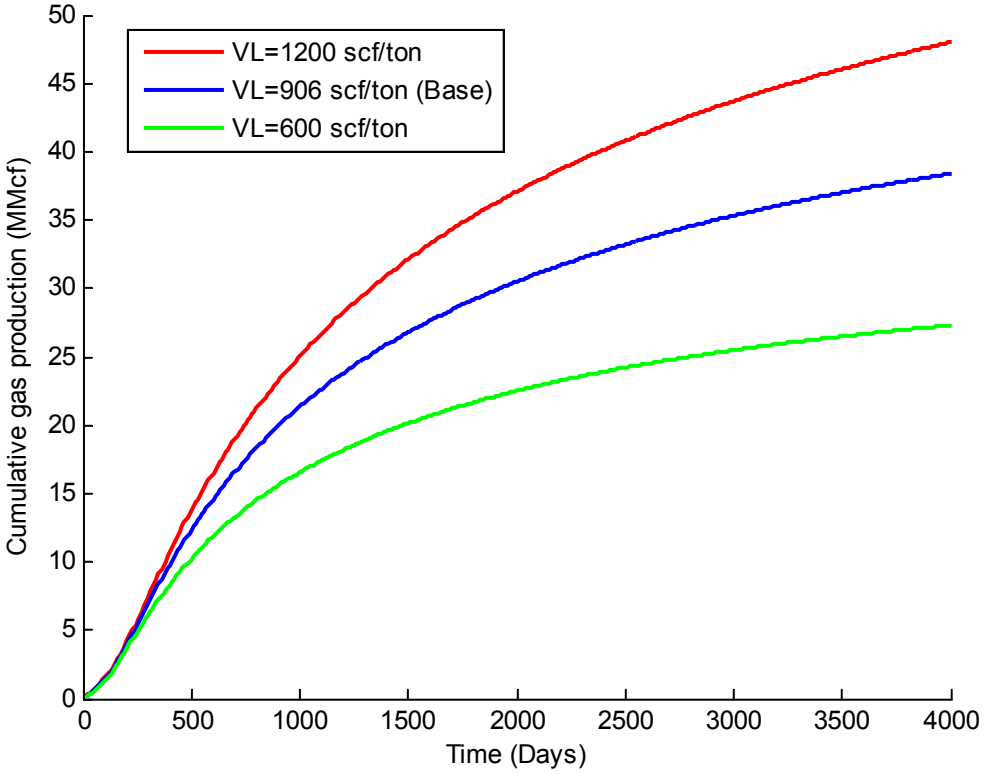

Figure 27 Cumulative gas production for different adsorption capacity

The blue line in Figure 26 is the result from base case (same as Figure 24). When the Langmuir Volume constant increases to 1200 scf/ton (red line), the peak gas rate will increase to around 340 Mcf/Day and the time to reach the maximum gas rate also increases slightly. This is because when the initial pressure is fixed, increase of producible gas volume accompanies the increase of gas sorption capacity. It will provide more gas supply to maintain higher production rate and postpone the decline effect. In addition, at early stage (in this case is about before 300 days), the production rate profile and cumulative production (Figure 27) have the same trend for different Langmuir Volume constant, which is because the free phase gas plays a much more important roles than the desorption gas in this stage.

5.4 Effect of Multi-mechanistic gas flow

Transportation of gas in the reservoir could be influenced by pressure and concentration gradients simultaneously. The gas flow in fracture domain is under the pressure field and obeys the Darcy's law while the gas flow in matrix domain is under concentration field and obeys the Fick's law of diffusion. We had done several cases with different diffusion coefficients range from 10^{-7} to 10^{-3} to investigate the multi-mechanistic flow of gas in permeable, tight, and ultra-tight system. And we also compared all these result with the case have diffusion coefficient of 0 which represents the single-mechanistic flow (Darcy flow) to show how diffusion flow affect the production flowrate prsofile. The parameters to separate three different systems are fracture permeability and matrix permeability values. Table 9 and Figure 8 list all the parameters used in these cases. Figure 28-Figure 30 summarize the gas production rate for the reservoir with different diffusion coefficients.

Table 9 Input variables for sensitivity analysis of multi-mechanistic flow in permeable and tight system

Parameters	Permeable system	Tight system	Ultra tight system	units
Reservoir size	1100x1100	1100x1100	1100x1100	ft
Reservoir thickness	20	20	20	ft
Fracture porosity	1	1	1	%
Matrix porosity	8	8	8	%
Fracture permeability	1000	5	0.1	md
Matrix permeability	1	0.005	0.0001	md
Initial pressure	1100	1100	1100	psia
Fracture spacing	0.01	0.01	0.01	ft
Initial water saturation, fracture	95	95	95	%
Initial water saturation, matrix	70	70	70	%
Irreducible water saturation	20	20	20	%
Reservoir temperature	100	100	100	°F

Number of grid blocks	11,11,1	11,11,1	11,11,1	-
Well location	6,6,1	6,6,1	6,6,1	-
Well radius	0.25	0.25	0.25	ft
Sandface pressure	100	100	100	psia
Skin factor	0	0	0	-
Coal density	1.435	1.435	1.435	g/cm
Langmuir volume	906	906	906	SCF/ton
Langmuir pressure	625	625	625	psia
Diffusion coefficient	0,10^{-3}, 10^{-5}, 10^{-7}	0,10^{-3}, 10^{-5}, 10^{-7}	0,10^{-3}, 10^{-5}, 10^{-7}	ft/day

Permeable reservoirs

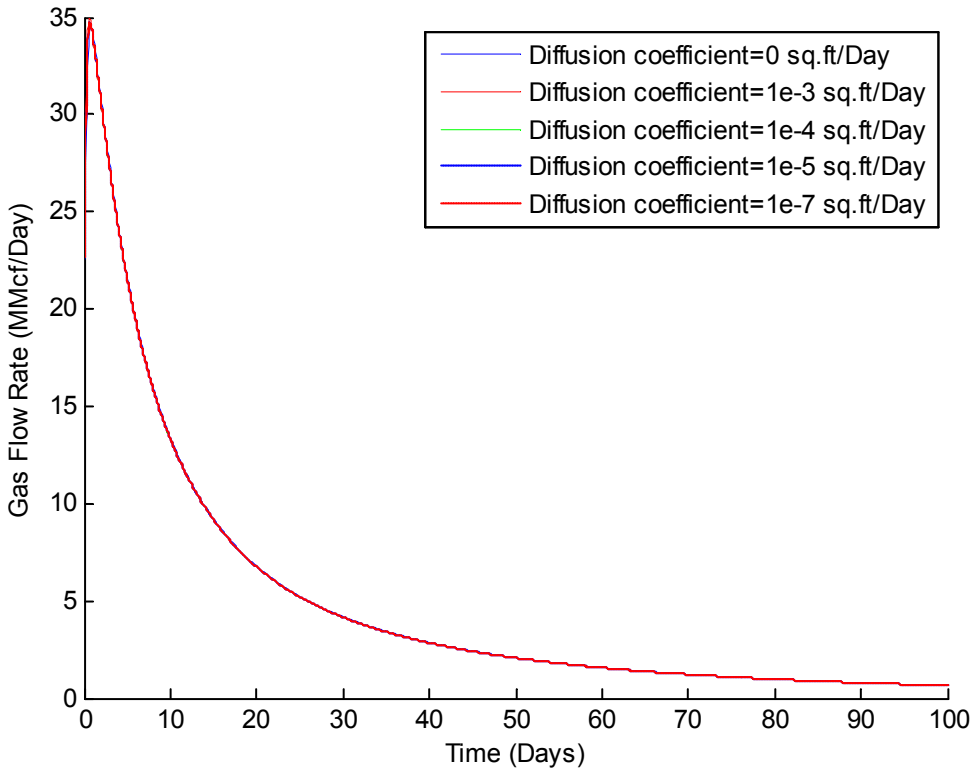

Figure 28 Gas production profile with different diffusion coefficient in permeable reservoir

Figure 28 shows that the gas production rate are almost the same even they had different diffusion coefficients in permeable system, where fracture permeability is 1000 md and matrix

permeability is 1 md. Since both of them are high enough to be the case that Darcian flow dominates. Diffusion flow still exist in the system, but it is negligible. Therefore, diffusion does not have significant effect on the production profile in permeable system.

Tight reservoir

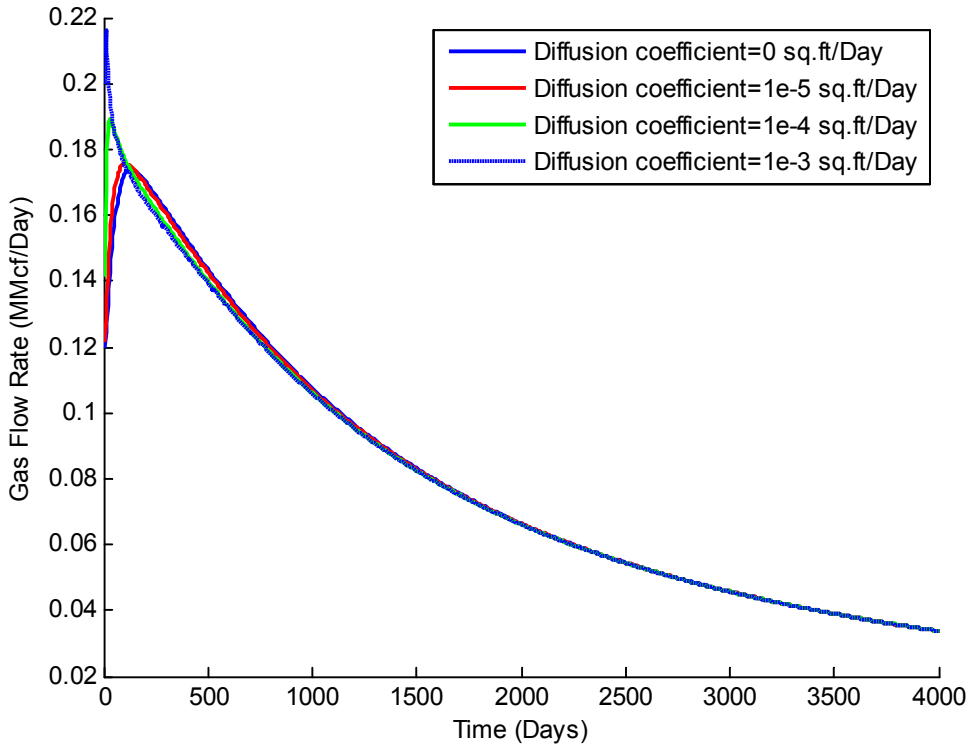

Figure 29 Gas production profile with different diffusion coefficient in tight reservoir

Figure 29 shows the gas production rate in tight reservoir with different diffusion coefficients. It could be observed that the diffusion flow becomes more dominant in this case than in permeable reservoir. The initial gas flow rate is higher when the reservoir with larger diffusion coefficient. In addition, the time to reach maximum production rate become shorter when the diffusion coefficient increase, which means at each time step the matrix will release more gas to the fracture then to the wellbore. Moreover, comparing y axis with previous case, the

gas flow rate decrease significantly because the permeability in fracture and matrix both decreased.

Ultra-tight reservoir

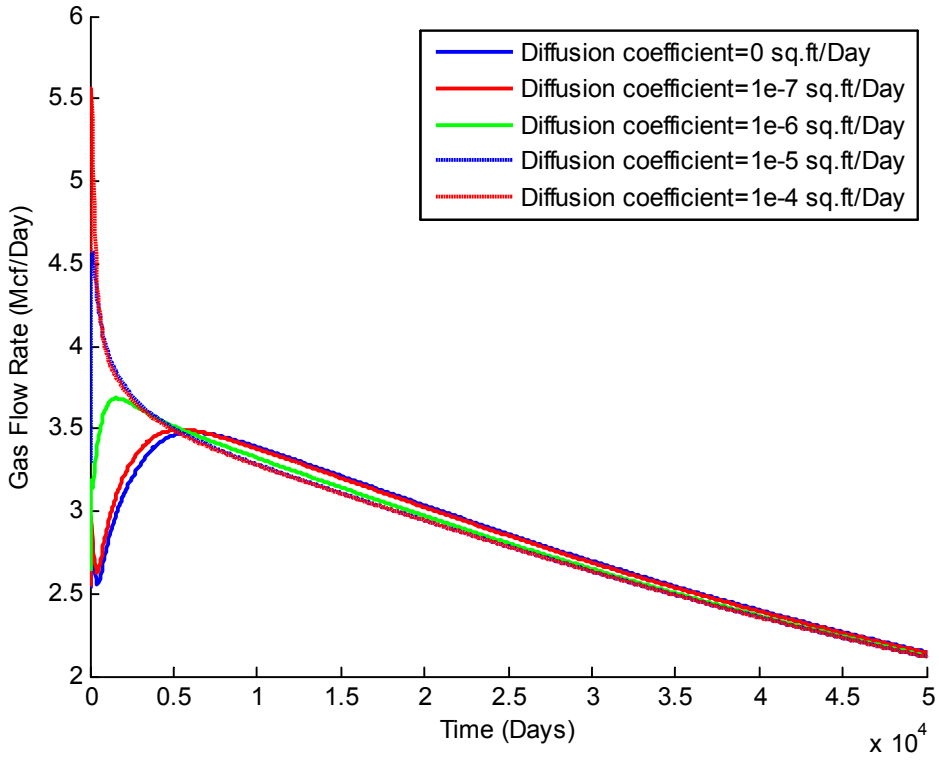

Figure 30 Gas production profile with different diffusion coefficient in ultra-tight reservoir

Figure 30 indicates the gas flow rate in ultra-tight reservoir with different diffusion coefficients. It could be illustrated that the Fickian flow become much more dominant than previous two. Since both fracture and matrix permeability decrease, the order of the production rate also decrease a lot and production period to have a similar trend which will take longer as 50000 days.

In a summary, the diffusion has larger effect on the gas production rate as the permeability of fracture and matrix become lower, which also means the diffusion flow rate become more dominant.

5.5 Effect of cleat spacing

CBM reservoir is a naturally fractured reservoir. Therefore, clear spacing will also be one of the important parameters affecting the gas flowrate and cumulative production. The cleat spacing is coupled inside the shape factor as we mentioned in section 3.4. The shape factor controlled the mass transfer between fracture domain and matrix domain, and affect the amount of both Darcian flow and diffusion flow (equation 3.36). Table 10 listed all the parameters used in this simulation case. Cleat spacing is the only variable in these cases. Since we want to show not only the sensitivity analysis in CBM reservoirs, but also to prove the capability of this model. So we had tested 0.1ft, 1ft, and 10ft for fracture spacing, even if 10ft is much larger than the reasonable range of CBM reservoir fracture spacing.

Table 10 Input parameters of sensitivity test with different fracture spacing of the reservoir

Parameters	Dual-ϕ dual-k	units
Reservoir size	1100x1100	ft
Reservoir thickness	20	ft
Fracture porosity	0.1	%
Matrix porosity	0.5	%
Fracture permeability	10	md
Matrix permeability	0.005	md
Initial pressure	1100	psia
Fracture spacing	0.1, 1, 10	ft
Initial water saturation, fracture	95	%
Initial water saturation, matrix	40	%
Irreducible water saturation	20	%
Reservoir temperature	114	°F
Number of grid blocks	11,11,1	-
Well location	6,6,1	-
Well radius	0.25	ft
Sandface pressure	14.7	psia
Skin factor	0	-
Coal density	1.435	g/cm
Langmuir volume	906	SCF/ton
Langmuir pressure	625	psia

Diffusion coefficient	1.00E-07	ft^2/day

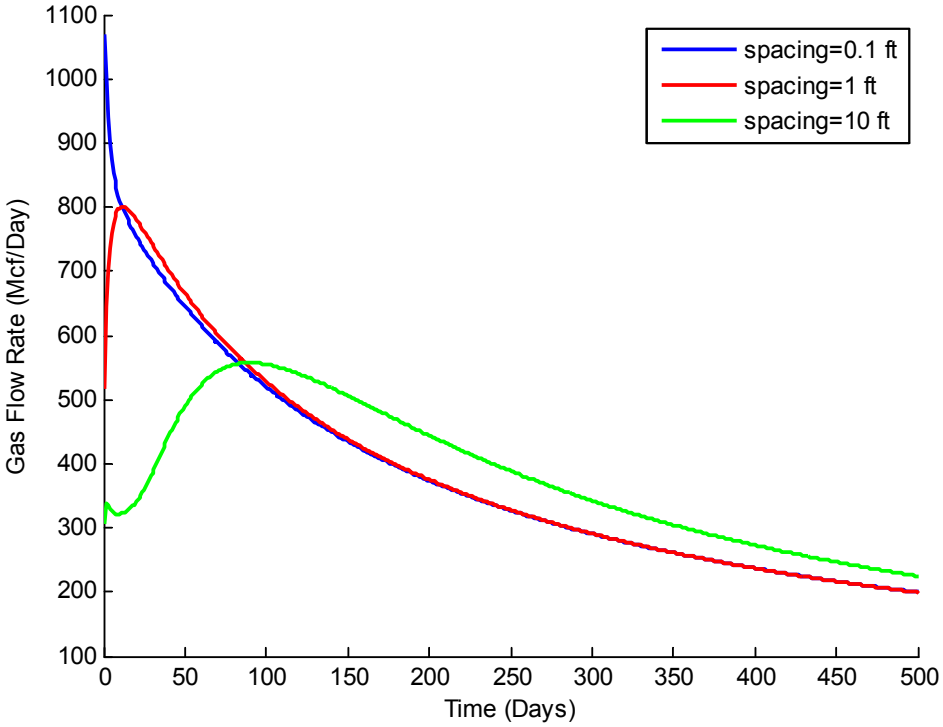

Figure 31 Evolution of gas production rate under different fracture spacing of the reservoir

Figure 31 described the gas production rate results with different fracture spacing. When the fracture spacing is small as 0.1ft, which means we have more fractures in the reservoir, the initial gas flowrate is around 1100 Mcf/Day. The initial gas flowrate decreased when the fracture spacing became larger. In addition, the amount of maximum gas rate also decreased with the increased fracture spacing. However, the time to reach the gas production peak rate has the opposite trend which means it will take longer time when fracture spacing increase. The reason is that the mass exchange between two systems becomes slower when the fracture spacing becomes larger.

5.6 Effect of initial gas content

The degree of gas saturation is also one of the important parameter in a CBM reservoir. As we discussed in Figure 5, if the initial coal reservoir conditions gas content and pressure fall on

the Langmuir isotherm line, the reservoir could be considered as saturated, and the gas will release from the matrix once lowering the pressure. However, in most of the CBM reservoirs, the initial gas content are not fully saturated as 100%. Therefore, when the reservoir starts to produce, it will only produce the free gas and water from the fracture and matrix pores. The gas will release from the matrix until the reservoir depressurized to the desorption pressure. Figure 32 is the Langmuir isotherm curve for this simulation, we had tested four different cases, 100%, 80%, 60%, and 40% capacity of initial gas content. All the parameters we used in these cases are the same as the base case except the percentage of initial gas content.

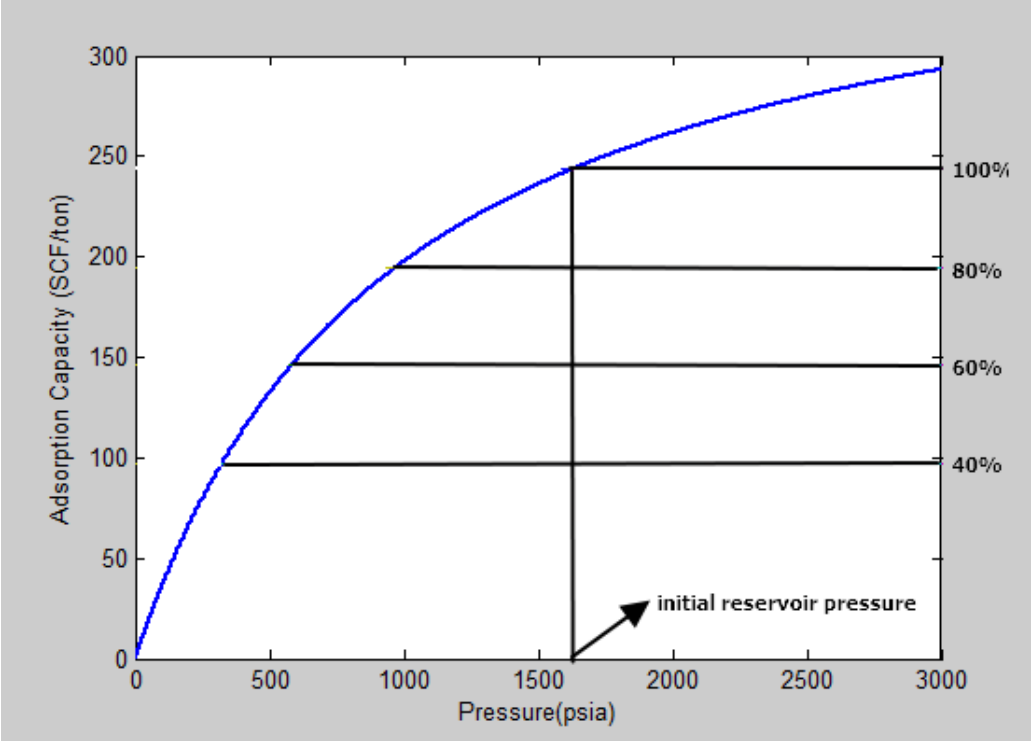

Figure 32 Methane sorption isotherm for sensitivity analysis case of undersaturated initial gas content (V_m=386.695 SCF/ton, P_m= 956.023 psia)

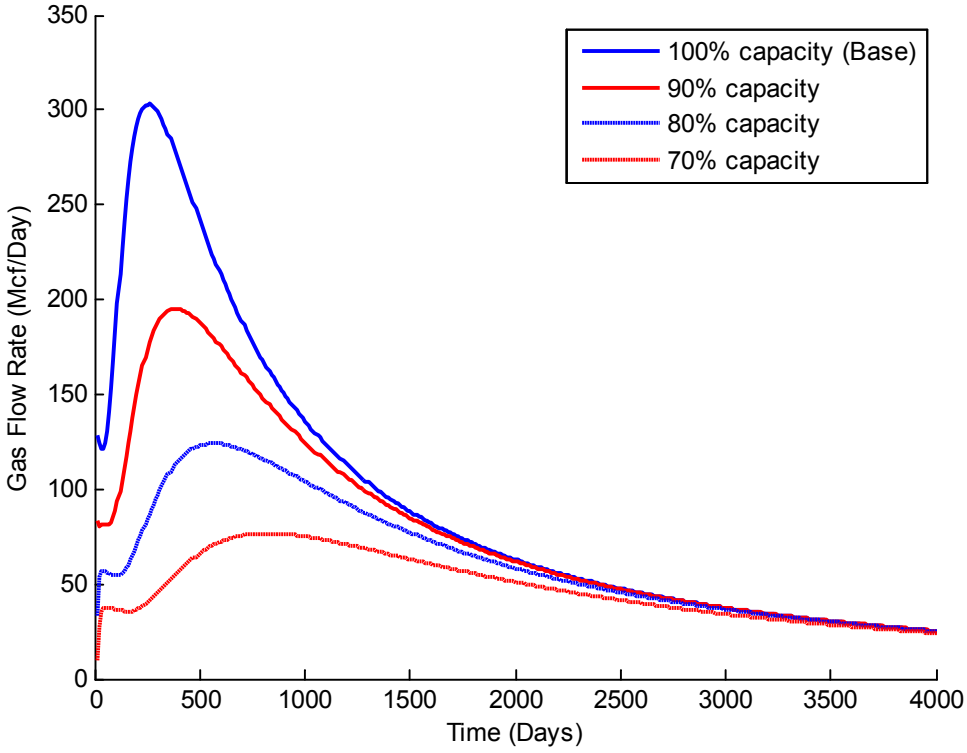

Figure 33 Gas production profile of sensitivity analysis case with different initial gas content

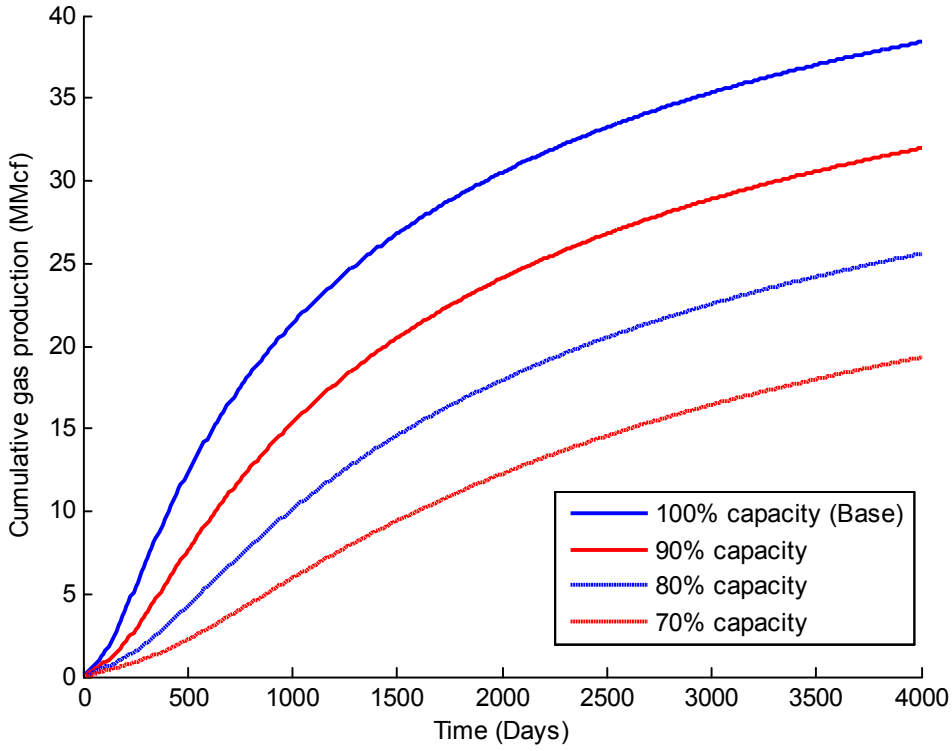

Figure 34 Cumulative gas production with different initial gas content

Figure 33 shows results of gas flowrate for all different cases. The results indicate that we will have higher peak gas production rate with higher initial gas content. We also reach the peak rate earlier when we have higher initial gas content in that the peak rate will happen after the gas starts to release from the matrix, which need the reservoir depressurize under the desorption pressure. In addition, Figure 34 indicates the cumulative gas production profile. It is easily to understand that we will have highest production with highest initial gas content in the field.

5.7 Effect of permeability evolution

Permeability evolution is a well-accepted phenomenon in CBM reservoir during depletion. Therefore, we had investigated several different permeability models, which including P&M, S&D, Thararoop, P&M&Liu, and S&D&Liu (Palmer and Mansoori 1998; Shi and Durucan 2005; Thararoop 2010; Liu and Harpalani 2013b). All these models had been discussed in chapter 2 and 3. In this section, we used all the data from several different literatures which studied for same area, San Juan Basin (Palmer and Mansoori 1998; Chen et al. 2013; Shi and Durucan 2005; Thararoop 2010; Hueni et al. 1990; Mavor, Owen, and Pratt 1990; Liu and Harpalani 2013b). Table 11 reported the input parameters we used in these cases. From the base case, the initial pressure is 1100 psia, so we plotted all the models from 1100 psia and below (Figure 35). The y-axis is the ratio between reservoir permeability and initial permeability and x-axis is the corresponding pressure. We can observe from the figure that P&M and Thararoop model first slight decrease and then become increasing for the permeability. This is because they believe at early stage the rock compression is dominant, so permeability decrease due to increased effective stress triumphs the permeability increase due to shrinkage resulting from the desorption. However, for P&M&Liu and S&D&Liu models, they believed that in the low pressure region, the permeability evolution is dominant by the desorption state and the permeability will only

increasing at this pressure range. Therefore, for these two models, permeability will only have increasing trend when we produce gas from the reservoir with the 1100 psia initial pressure.

In order to investigate the effect of permeability evolution due to the coal shrinkage when producing, all five models above had been coupled into our dual-porosity, dual-permeability model. All the setting for reservoir is same as the base case except we enlarge the reservoir size to 2200ft by 2200ft, which can let us produce for a longer time to have clear plots for the results.

Table 11 Input data for permeability evolution models

Parameters	value	unit
E	450000	psi
v	0.35	dimensionless
K	676400	psi
M	890000	psi
f	0.5	dimensionless
r	1.2962E-6	psi^{-1}
$\boldsymbol{\beta}$	0.0016	psi^{-1}
$\boldsymbol{\varepsilon_l}$	0.0128	dimensionless
$\boldsymbol{\alpha_S V_L}$	0.01266	scf
$\boldsymbol{\alpha_S}$	0.00038	ft^3/scf
EA	232060.4	psi
$\boldsymbol{C_f}$	0.00051	psi^{-1}
$\boldsymbol{\rho\beta V_m}$	0.00325	dimensionless
R	10.731	ft^3*psi/lbmol*R
$\boldsymbol{V_o}$	358.8176	ft^3/lbmol

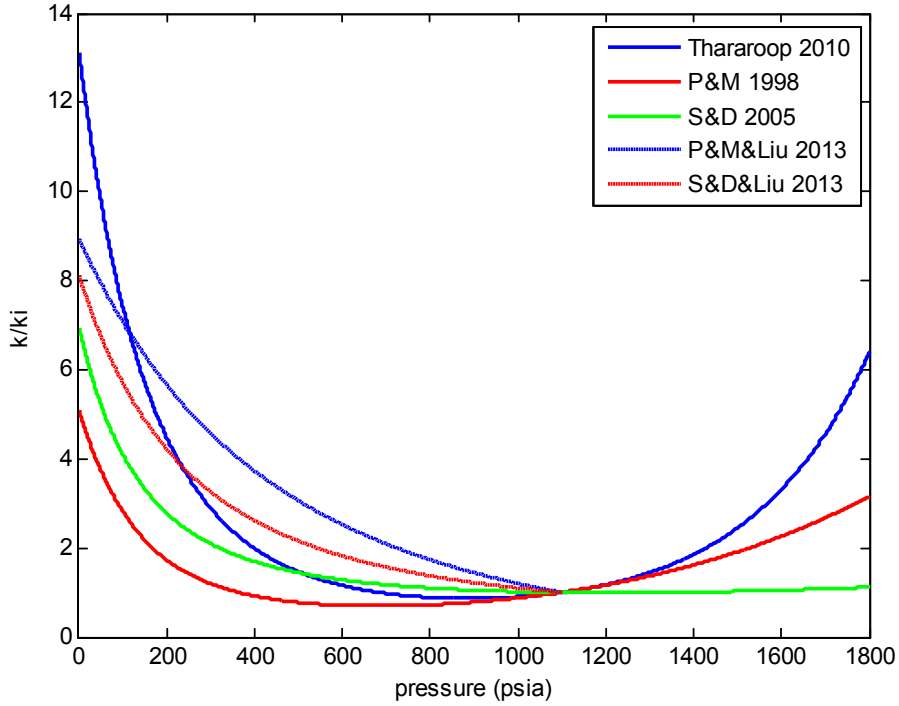

Figure 35 Plots of permeability evolution models for the targeting range

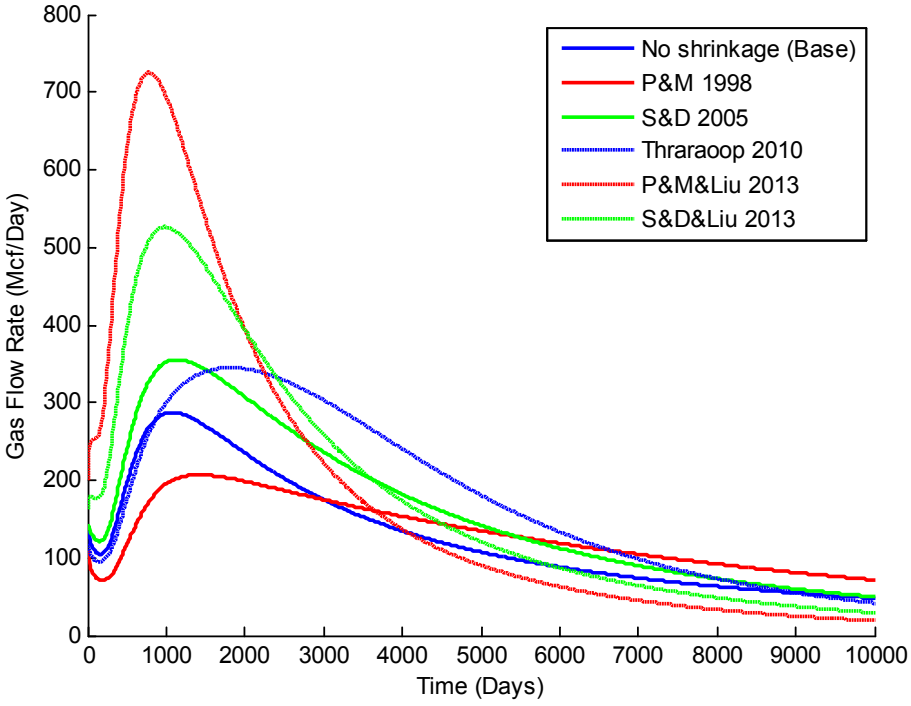

Figure 36 Gas production rate profile for different permeability evolution model

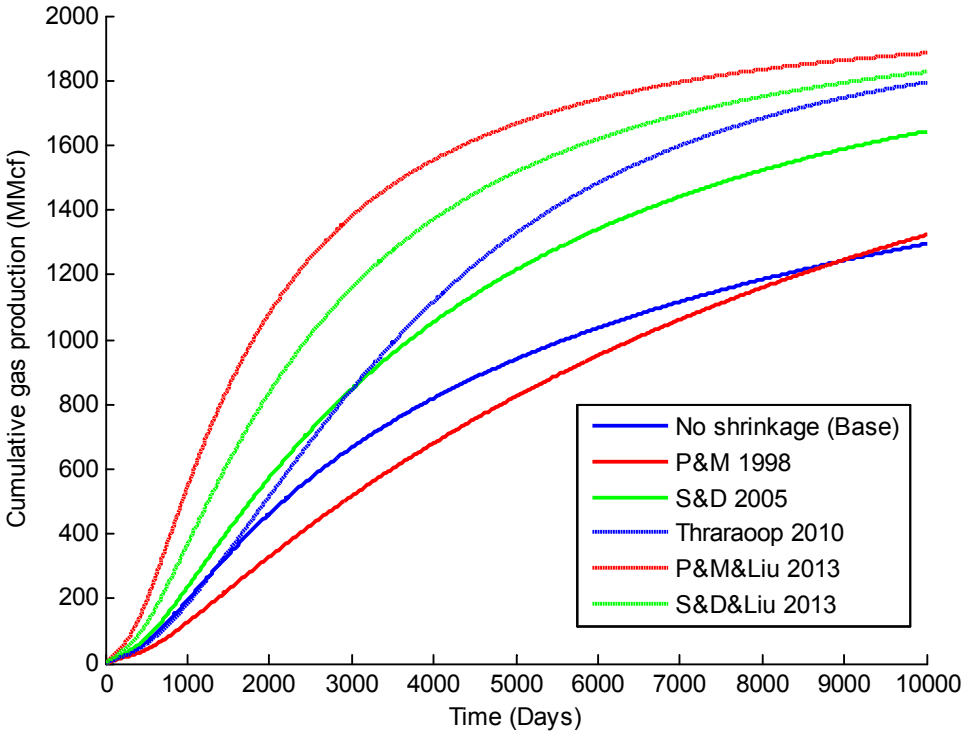

Figure 37 Cumulative gas production for different permeability evolution model

Figure 36 and Figure 37 show the gas flow rate profiles and cumulative gas production profiles. The highest peak flow rate is around 720 Mcf/Day and the lowest one is about 200 Mcf/Day. Comparing with the base case, the results showed a good agreement with the change in permeability. As we mentioned before, the P&M and Thararoop model had a slightly decrease at the beginning of the production process, so the production rate at early time will be lower than the base case and then became larger at the late period. The other three models only have the increasing trend when producing. Hence, they will have higher peak flow rate than the base case and lower production rate at the late time.

In addition, we use two different scenario to describe the permeability in matrix, first treat with the same physics as the permeability evolution in fracture system, and then treat as constant as the second case for all production period. We found that since the permeability in

matrix is a very small number, which in these two cases the effect on the production rate are the same.

5.8 Effect of dewatering operation

Most CBM wells go through a dewatering phase which might be months or even years. Permeability could increase or decrease during their operations. If dewater rate is too low, the pressure decrease not much, hence gas will not come out from the matrix. If dewater rate is too high, effective stress will increase soon and cause the cleat close and decrease the permeability. Therefore, we investigate different FBHP to see how it will affect the production. In the base case, sandface pressure was a constant set as 100 psia. In these section, sandface pressure are set to be 60%, 40%, and 20% of reservoir pressure. Figure 38 shows that the gas production rate increases with reducing sandface pressure. The rates in the order of increasing sandface pressure values are about 270 Mcf/Day, 170 Mcf/Day, and 90 Mcf/Day, respectively. But, we can observe from the figure that the time it took to reach the peak rate is almost the same.

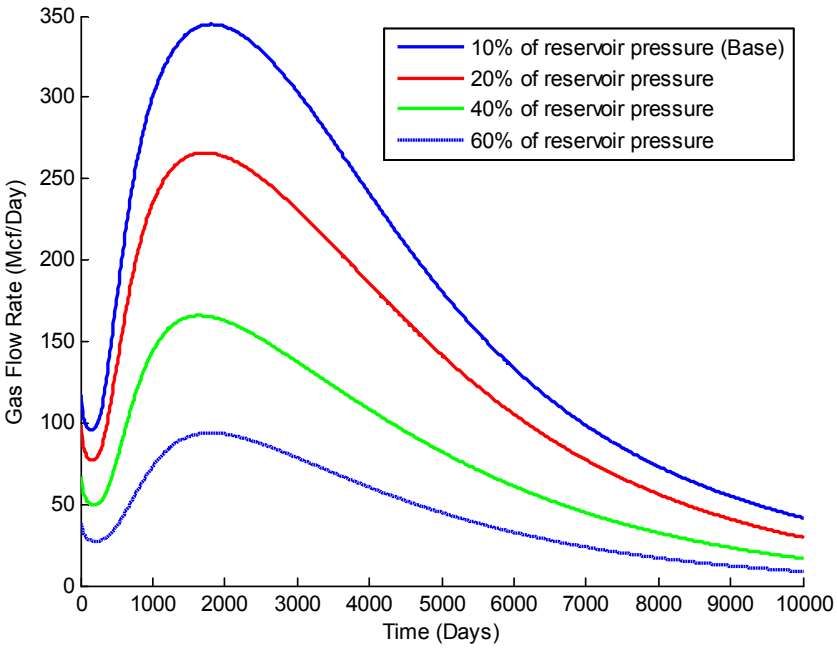

Figure 38 Gas production rates with different sandface pressure

5.9 Effect of hydraulic fracture

Hydraulic fracturing is one of the stimulation method to increase gas recovery from unconventional reservoirs. We set a bi-wing fracture treatment with different fracture half length (150, 250, 350 ft) and different fracture conductivity (50 md, 500 md, 5 Darcy, 50 Darcy) to see the impact on gas recovery rates. Figure 39 to Figure 44 are the results for different fracture half-length.

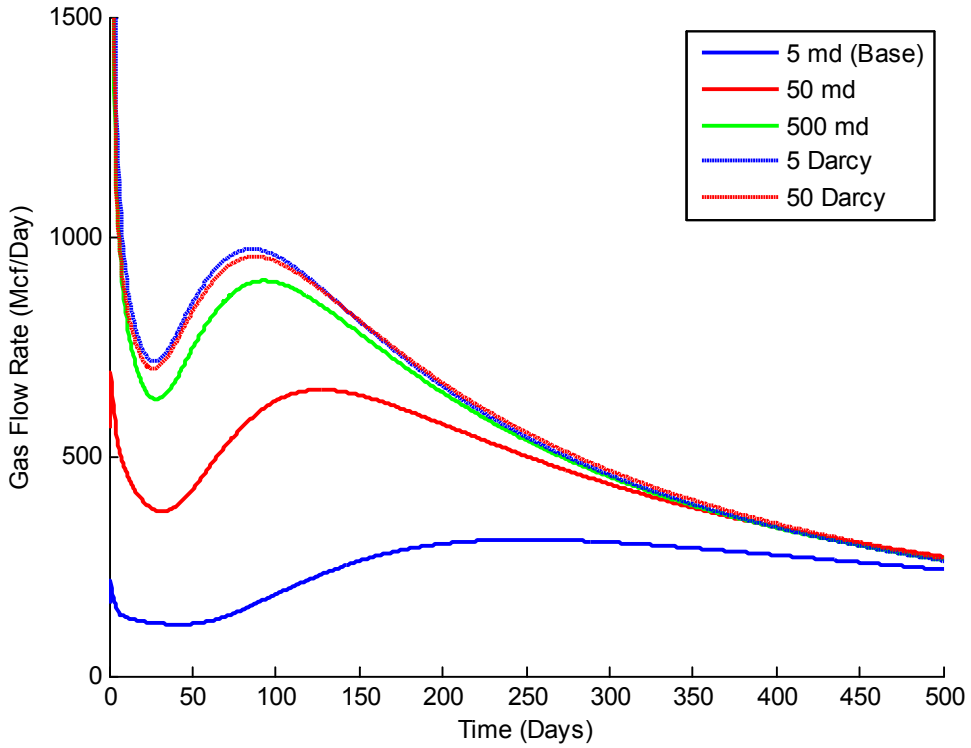

Figure 39 Gas production rates after fracture treatment (different fracture permeability) with $L_f = 150\ ft$

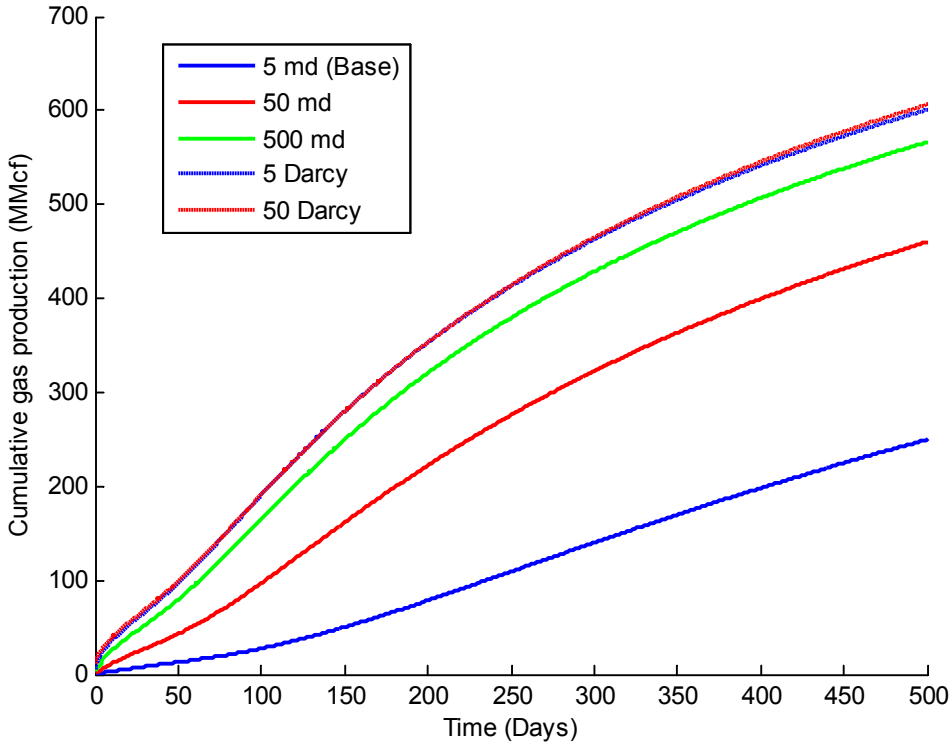

Figure 40 Cumulative gas production after fracture treatment (different fracture permeability) with $L_f = 150\ ft$

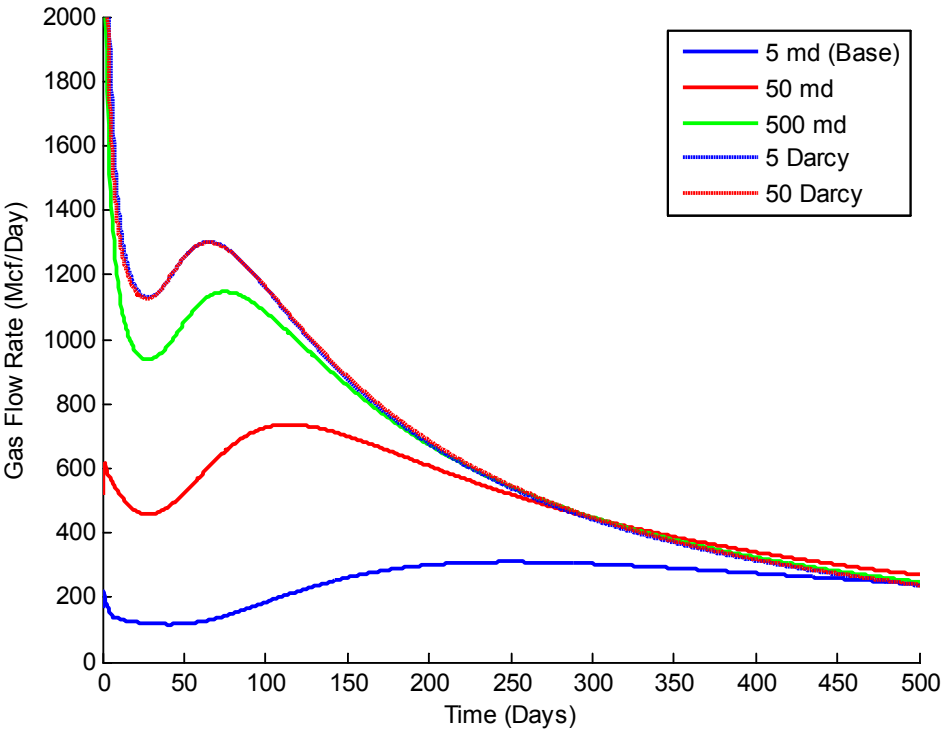

Figure 41 Gas production rates after fracture treatment (different fracture permeability) with $L_f = 250\ ft$

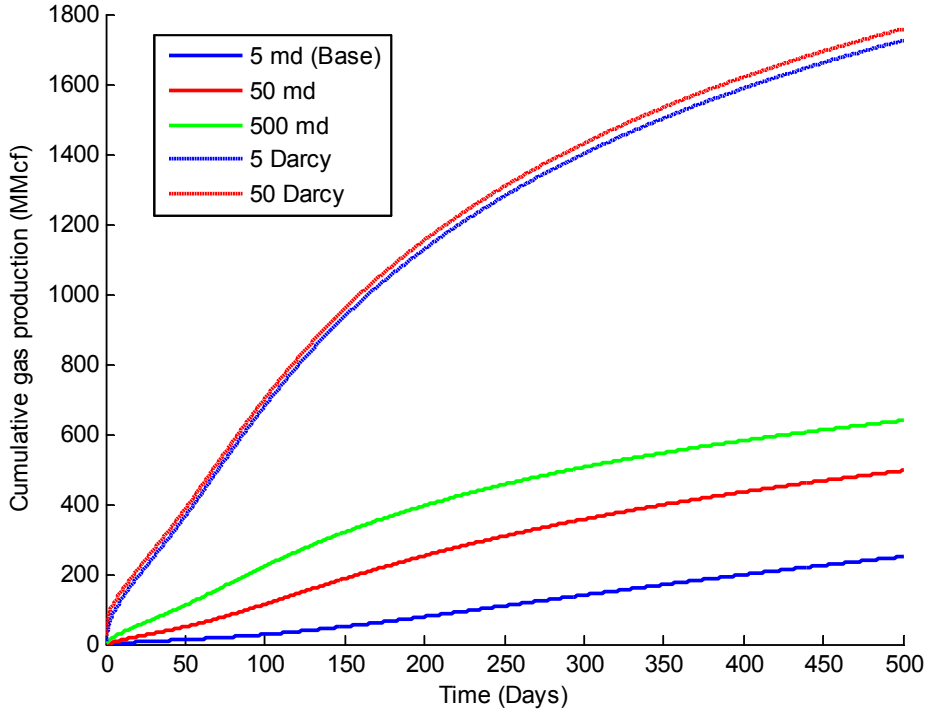

Figure 42 Cumulative gas production after fracture treatment (different fracture permeability) with $L_f = 250\ ft$

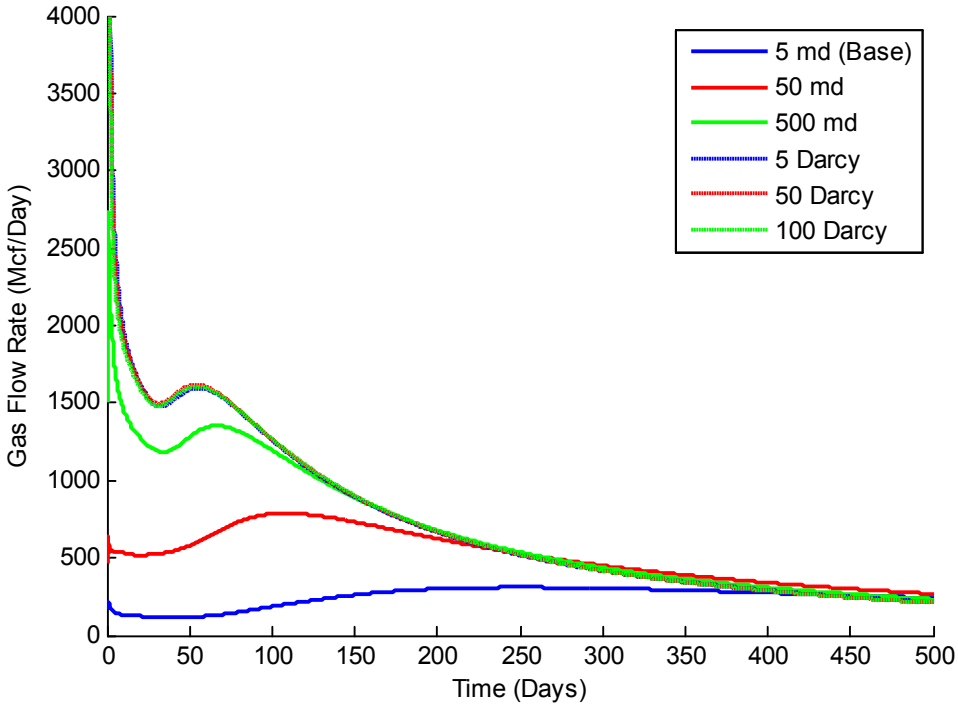

Figure 43 Gas production rates after fracture treatment (different fracture permeability) with $L_f = 350\ ft$

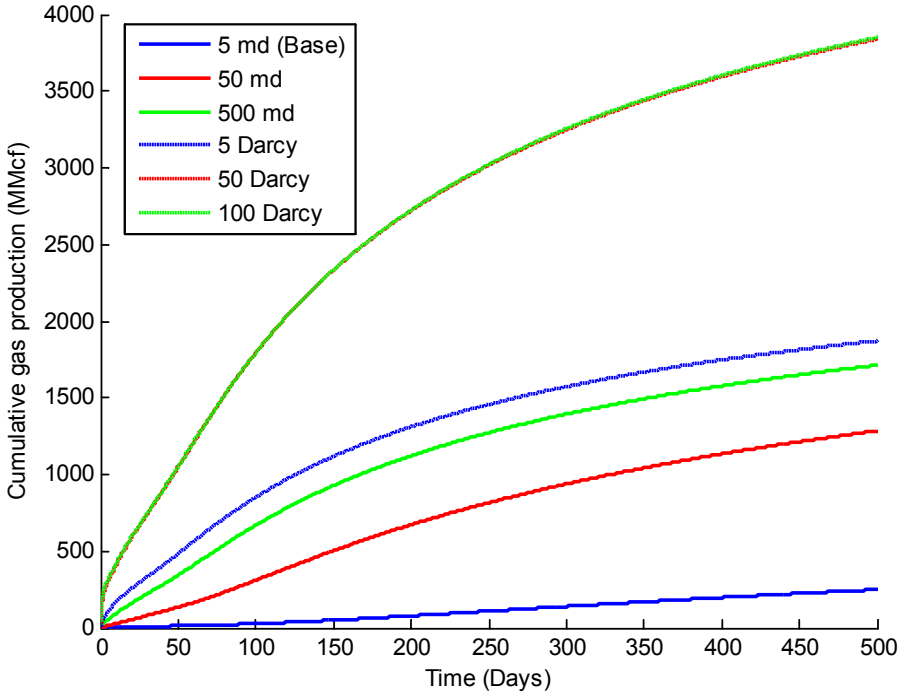

Figure 44 Cumulative gas production after fracture treatment (different fracture permeability) with $L_f = 350\ ft$

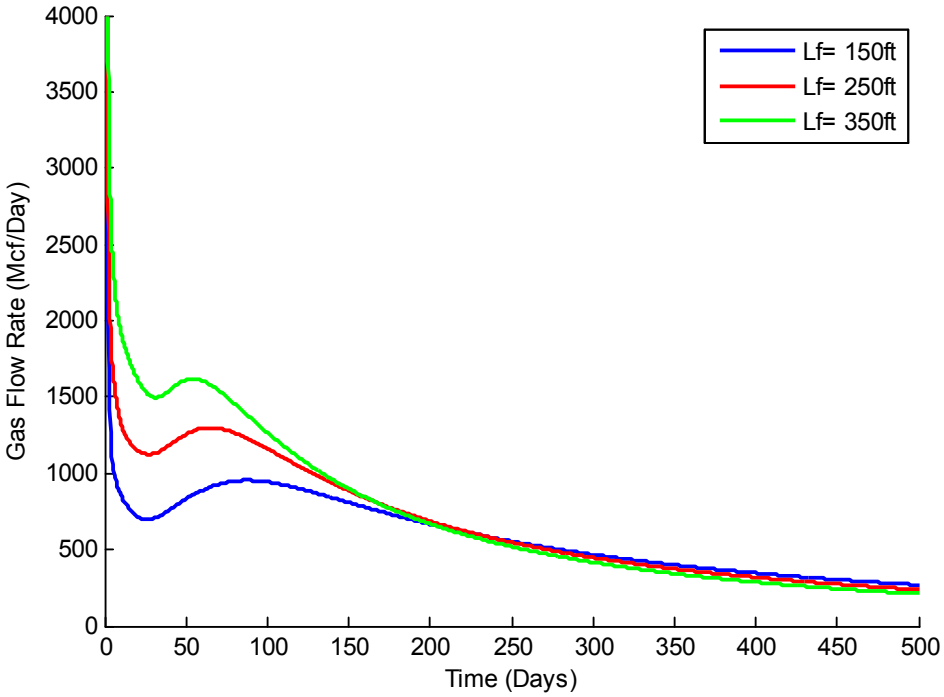

Figure 45 Gas production rates after fracture treatment (different fracture half length) with permeability at 50 Darcy

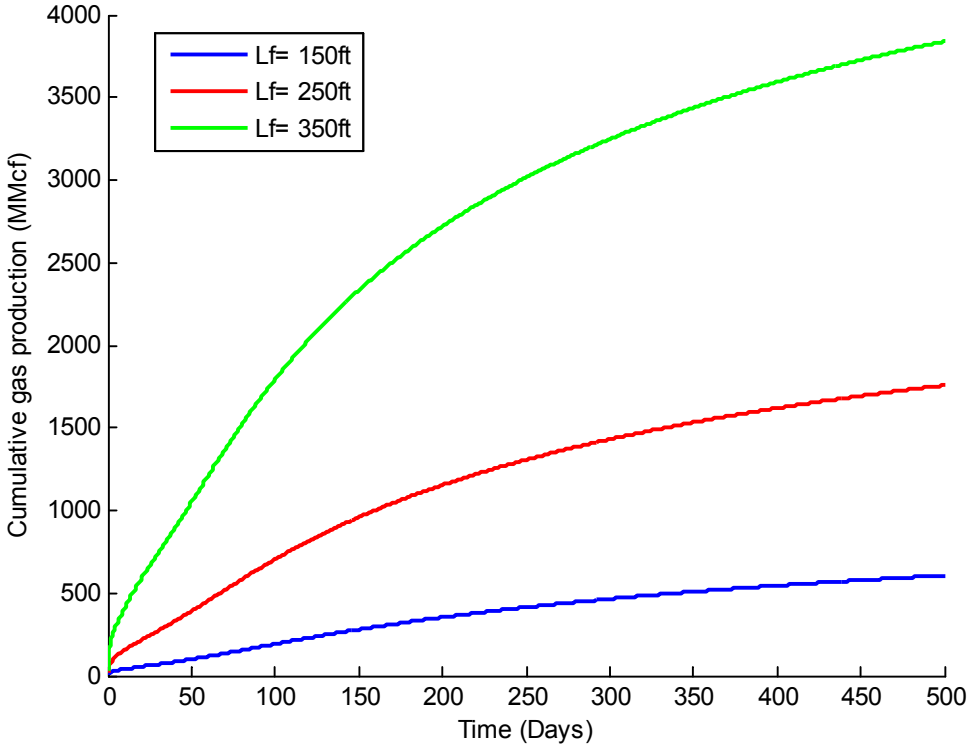

Figure 46 Cumulative gas production after fracture treatment (different fracture half length) with permeability at 50 Darcy

From Figure 39 and Figure 40, the fracture half-length is 150 ft, gas recovery and cumulative gas production increased with the permeability increased. However, the case with 5 Darcy and 50 Darcy had almost the same results. In these two case, the conductivity of hydraulic fracture treatment reached the limit. Hence, it is not worth to increase the hydraulic fracture to 50 Darcy, but we can change the treatment to increase the fracture half-length which can further increase the total amount of recovery. This phenomenon could also been observed from the case with 250ft and 350ft as fracture half-length. Therefore, Figure 45 and Figure 46 show the results with same hydraulic fracture permeability but different fracture half length. The results indicates that the gas recovery rate and cumulative gas production increase with the fracture half-length increase.

Chapter 6 Conclusion

In this thesis, a 3-D, 2-phase, dual-porosity, dual permeability reservoir simulation model with permeability evolution had been built and validated. We also conducted a series of parametric studies to investigate the impact of all those parameters including effect of desorption, adsorption capacity, multi-mechanistic gas flow, cleat spacing, initial gas content, permeability evolution, dewater operations, and hydraulic fracture treatment. The conclusions are as follows:

1. Adsorption capacity of coal seam changes with coal ranks. Higher coal rank with higher adsorption capacity (Langmuir Volume constant) results in higher gas peak rate at a later time. When the adsorption capacity increased from 600 to 1,200 scf/ton, the gas peak rate increased 31 % from 256 to 337 Mcf/Day, but the cumulative gas production increased by 76%.
2. The diffusion flow has larger impact on gas recovery rate when fracture and matrix permeability are smaller than 5 md and 0.005 md, respectively, which also means the diffusion flow became more dominant than Darcian flow.
3. When the cleat spacing increases from 0.1 ft to 1 ft, the shape factor will become smaller and reduce the mass exchange between the fracture and matrix domain, which results in a decrease of gas production peak rate by 33%.
4. Undersaturated CBM reservoirs will decrease the gas production peak rate and also increase the time to reach the peak rate. A reservoir with initial gas content at 70% capacity could result in around half reserve in 10 years period.
5. We should choose the permeability evolution model carefully based on mechanics of coal and mechanism of flow since different model affect the gas recovery significantly.

6. Increased FBHP from 10% of reservoir pressure to 60% of reservoir pressure will result in a decrease cumulative gas production by 75%. However, with the combination of permeability evolution effect and the BHFP, using 40% of initial reservoir pressure is the optimum method in our case.
7. A successful fracturing treatment could increase the cumulative gas production by 2-8 times larger.

With capture all these effects in the model and the analysis of these impact factors, our model could be an efficient engineering tool to analyze the CBM reservoir and further predict the gas production performance.

References

Balan, Huseyin Onur, and Fevzi Gumrah. 2009. "Assessment of Shrinkage–swelling Influences in Coal Seams Using Rank-Dependent Physical Coal Properties." *International Journal of Coal Geology* 77 (1-2). Elsevier B.V.: 203–13. doi:10.1016/j.coal.2008.09.014.

Bell, J.S. 2006. "In-Situ Stress and Coal Bed Methane Potential in Western Canada." *BULLETIN OF CANADIAN PETROLEUM GEOLOGY* 54 (3): 197–220.

Ceglarska-Stefańska, Graiyna, and Kinga Brzóska. 1998. "The Effect of Coal Metamorphism Methane Desorption." *Fuel* 77 (6): 645–48.

Ceglarsk-Stefańska, G., and K. Zarębska. 2002. "The Competitive Sorption of CO 2 and CH 4 with Regard to the Release of Methane from Coal." *Fuel Processing Technology* 77-78: 423–29.

Chakhmakhchev, Alex. 2007. "Worldwide Coalbed Methane Overview." *Society of Petroleum Engineers*, 1–7.

Chang, Ming-Ming. 1993. "Deriving the Shape Factor of a Fractured Rock Matrix."

Chawathe, A, Petroleum Recovery, T Ertekin, The Pennsylvania State, and A Grader. 1996. "Understanding Multimechanistic Gas-Water Flow in Fractured Reservoirs: Mapping of the Multimechanistic Flow Domain," no. 1.

Chen, Zhongwei, Jishan Liu, Akim Kabir, Jianguo Wang, and Zhejun Pan. 2013. "Impact of Various Parameters on the Production of Coalbed Methane."

Coats, K.H. 1989. "Implicit Compositional Simulation of Single-Porosity and Dual-Porosity Reservoirs." *SPE Symposium on Reservoir Simulation*, April. Society of Petroleum Engineers. doi:10.2118/18427-MS.

Durucan, Sevket, Mustafa Ahsanb, and Ji-Quan Shia. 2009. "Matrix Shrinkage and Swelling Characteristics of European Coals." *Energy Procedia* 1 (1). Elsevier: 3055–62. doi:10.1016/j.egypro.2009.02.084.

Ertekin, Turgay, Gregory A. King, and Fred C. Schwerer. 1986. "Dynamic Gas Slippage : A Unique Dual · Mechanism Approach to the Flow of Gas in Tight Formations." *Society of Petroleum Engineers Journal* 1 (01): 43–52. doi:http://dx.doi.org/10.2118/12045-PA.

Fick, A. 1855. "On Liquid Diffusion." *Philosophical Magazine* 10: 30–39.

Harpalani, S, and R Schraufnagel. 1990. "Shrinkage of Coal Matrix with Release of Gas and Its Impact on Permeability of Coal." *Fuel* 69 (5): 551–56. doi:10.1016/0016-2361(90)90137-F.

Harpalani, Satya. 1984. "Gas Flow Through Stressed Coal." *Ph.D Thesis*.

Hueni, G B, R E Jones, Jerry R Bergeson, K M Fitzgerald, and Mallon Oil Co. 1990. "The Gavilan Field: Inverse Rate Sensitivity in Dual-Porosity Reservoirs."

Kazemi, H., L.S. Merrill, K.L. Porterfield, and P.R. Zeman. 1976. "Numerical Simulation of Water-Oil Flow in Naturally Fractured Reservoirs." *SPE*.

Laubach, S.E, R.a Marrett, J.E Olson, and a.R Scott. 1998. "Characteristics and Origins of Coal Cleat: A Review." *International Journal of Coal Geology* 35 (1-4): 175–207. doi:10.1016/S0166-5162(97)00012-8.

Lim, K T, and K Aziz. 1995. "Matrix-Fracture Transfer Shape Factors for Dual-Porosity Simulators," no. 1989.

Liu, Shimin, and Satya Harpalani. 2013a. “A New Theoretical Approach to Model Sorption-Induced Coal Shrinkage or Swelling.” *AAPG Bulletin* 97 (7): 1033–49. doi:10.1306/12181212061.

———. 2013b. “Permeability Prediction of Coalbed Methane Reservoirs during Primary Depletion.” *International Journal of Coal Geology* 113 (July). Elsevier B.V.: 1–10. doi:10.1016/j.coal.2013.03.010.

Mares, Tennille E., Andrzej P. Radliński, Tim a. Moore, David Cookson, P. Thiyagarajan, Jan Ilavsky, and Jürgen Klepp. 2009. “Assessing the Potential for CO2 Adsorption in a Subbituminous Coal, Huntly Coalfield, New Zealand, Using Small Angle Scattering Techniques.” *International Journal of Coal Geology* 77 (1-2): 54–68. doi:10.1016/j.coal.2008.07.007.

Mavor, M.J., L.B. Owen, and T.J. Pratt. 1990. “Measurement and Evaluation of Coal Sorption Isotherm Data.” *SPE Annual Technical Conference and Exhibition*, April. Society of Petroleum Engineers, 1–14. doi:10.2118/20728-MS.

Mazumder, Saikat, Michael Scott, and Jessica Jiang. 2012. “Permeability Increase in Bowen Basin Coal as a Result of Matrix Shrinkage during Primary Depletion.” *International Journal of Coal Geology* 96-97 (July). Elsevier B.V.: 109–19. doi:10.1016/j.coal.2012.02.006.

Meng, Zhaoping, Jincai Zhang, and Rui Wang. 2011. “In-Situ Stress, Pore Pressure and Stress-Dependent Permeability in the Southern Qinshui Basin.” *International Journal of Rock Mechanics and Mining Sciences* 48 (1). Elsevier: 122–31. doi:10.1016/j.ijrmms.2010.10.003.

Milewska-duda, Janina, Jan Duda, Adam Nodzen, and Janos Lakatos. 2000. “Absorption and Adsorption of Methane and Carbon Dioxide in Hard Coal and Active Carbon.” *Langmuir* 16 (12): 5458–66.

Moore, Tim a. 2012. “Coalbed Methane: A Review.” *International Journal of Coal Geology* 101 (November). Elsevier B.V.: 36–81. doi:10.1016/j.coal.2012.05.011.

Palmer, Ian, and John Mansoori. 1996. “How Permeability Depends on Stress and Pore Pressure in Coalbeds--A New Model.” *SPE*.

———. 1998. “How Permeability Depends on Stress and Pore Pressure in Coalbeds : A New Model.” *Society of Petroleum Engineers* 1 (06): 539–44. doi:http://dx.doi.org/10.2118/52607-PA.

Pan, Zhejun, and Luke D. Connell. 2007. “A Theoretical Model for Gas Adsorption-Induced Coal Swelling.” *International Journal of Coal Geology* 69 (4): 243–52. doi:10.1016/j.coal.2006.04.006.

———. 2009. “Comparison of Adsorption Models in Reservoir Simulation of Enhanced Coalbed Methane Recovery and CO2 Sequestration in Coal.” *International Journal of Greenhouse Gas Control* 3 (1): 77–89. doi:10.1016/j.ijggc.2008.05.004.

———. 2011. “Modelling of Anisotropic Coal Swelling and Its Impact on Permeability Behaviour for Primary and Enhanced Coalbed Methane Recovery.” *International Journal of Coal Geology* 85 (3-4). Elsevier B.V.: 257–67. doi:10.1016/j.coal.2010.12.003.

———. 2012. “Modelling Permeability for Coal Reservoirs: A Review of Analytical Models and Testing Data.” *International Journal of Coal Geology* 92 (March). Elsevier B.V.: 1–44. doi:10.1016/j.coal.2011.12.009.

Radlinski, a.P, M Mastalerz, a.L Hinde, M Hainbuchner, H Rauch, M Baron, J.S Lin, L Fan, and P Thiyagarajan. 2004. “Application of SAXS and SANS in Evaluation of Porosity, Pore Size Distribution and Surface Area of Coal.” *International Journal of Coal Geology* 59 (3-4): 245–71. doi:10.1016/j.coal.2004.03.002.

Shi, Ji-quan, and Sevket Durucan. 2005. “A Model for Changes in Coalbed Permeability During Primary and Enhanced Methane Recovery.” *Society of Petroleum Engineers Journal* 8 (04): 291–99. doi:http://dx.doi.org/10.2118/87230-PA.

Somerton, W.H., I.M. Soylemezoglu, and R.C. Dudley. 1975. “Effect of Stress on Permeability of Coal.” *International Journal of Rock Mechanics and Mining Sciences & Geomechanics Abstracts* 12 (cm): 129–45. doi:10.1016/0148-9062(75)91244-9.

Sparks, D. P., T. H. McLendon, J. L. Saulsberry, and S. W. Lambert. 1995. “The Effects of Stress on Coalbed Reservoir Performance, Black Warrior Basin, U.S.A.” *Society of Petroleum Engineers*, 339–51.

St. George, J.D, and M.a Barakat. 2001. “The Change in Effective Stress Associated with Shrinkage from Gas Desorption in Coal.” *International Journal of Coal Geology* 45 (2-3): 105–13. doi:10.1016/S0166-5162(00)00026-4.

Tao, Shu, Yanbin Wang, Dazhen Tang, Hao Xu, Yumin Lv, Wei He, and Yong Li. 2012. “Dynamic Variation Effects of Coal Permeability during the Coalbed Methane Development Process in the Qinshui Basin, China.” *International Journal of Coal Geology* 93 (April). Elsevier B.V.: 16–22. doi:10.1016/j.coal.2012.01.006.

Thararoop, Prob. 2010. “DEVELOPMENT OF A MULTI-MECHANISTIC, DUAL-POROSITY, DUAL-PERMEABILITY NUMERICAL FLOW MODEL FOR COALBED METHANE RESERVOIRS ACCOUNTING FOR COAL SHRINKAGE AND SWELLING EFFECTS.” The Pennsylvania State University.

Thararoop, Prob, Zuleima T. Karpyn, and Turgay Ertekin. 2009. “Development of a Coal Shrinkage – Swelling Model Accounting for Water Content in the Micropores Prob Thararoop * Turgay Ertekin.” *Int. J. Mining and Mineral Engineering* 1 (4): 346–64.

Wang, G.X., X.R. Wei, K. Wang, P. Massarotto, and V. Rudolph. 2010. “Sorption-Induced Swelling/shrinkage and Permeability of Coal under Stressed Adsorption/desorption Conditions.” *International Journal of Coal Geology* 83 (1). Elsevier B.V.: 46–54. doi:10.1016/j.coal.2010.03.001.

Warren, J.E., and P.J. Root. 1963. “The Behavior of Naturally Fractured Reservoirs.” *Society of Petroleum Engineers Journal* 3 (03): 245–55. doi:10.2118/426-PA.

Yao, Yanbin, Dameng Liu, Dazhen Tang, Shuheng Tang, Yao Che, and Wenhui Huang. 2009. “Preliminary Evaluation of the Coalbed Methane Production Potential and Its Geological Controls in the Weibei Coalfield, Southeastern Ordos Basin, China.” *International Journal of Coal Geology* 78 (1). Elsevier B.V.: 1–15. doi:10.1016/j.coal.2008.09.011.